A.R.A.P. Report No. 331

ATMOSPHERIC - WAKE

VORTEX INTERACTIONS

Alan J. Bilanin, Joel E. Hirsh,

Milton E. Teske and Arthur M. Hecht

Prepared under Contract No. NAS1-14707

by

Aeronautical Research Associates of Princeton, Inc.
50 Washington Road, P.O. Box 2229
Princeton, New Jersey

for

National Aeronautics and Space Administration
Langley Research Center
Hampton, Virginia 23665

February 1978

ATMOSPHERIC-WAKE VORTEX INTERACTIONS

Alan J. Bilanin, Joel E. Hirsh, Milton E. Teske
and Arthur M. Hecht

Aeronautical Research Associates of Princeton, Inc.
50 Washington Road, P.O. Box 2229
Princeton, New Jersey 08540

SUMMARY

The interactions of a vortex wake with a turbulent stratified atmosphere are investigated with the computer code "WAKE." It is shown that atmospheric shear, turbulence, and stratification can provide the dominant mechanisms by which vortex wakes decay.

Computations have included the interaction of a vortex wake with a viscous ground plane. Here, the observed phenomenon of vortex bounce is explained in terms of secondary vorticity produced on the ground. This vorticity is swept off the ground and advected about the vortex pair, thereby altering the classic hyperbolic trajectory. When compared with the decay of a vortex pair out of ground plane interaction, it is shown that strength of the vortex pair is rapidly reduced by the scrubbing on the ground.

The phenomenon of the solitary vortex is explained as an interaction of a vortex with crosswind shear. Here, the vortex having the sign opposite that of the sign of the vorticity in the shear is dispersed by a convective instability. This instability results in the rapid production of turbulence which in turn disperses the smoke marking the vortex.

It is shown that the effect of stable stratification on the descent of a vortex pair is to halt the descent of the pair. Numerical experiments have allowed a simple relation to be derived which predicts the maximum descent of a vortex pair in a linearly stratified atmosphere.

Lastly, the "WAKE" code has been updated, including new algorithms to improve accuracy and speed. In particular, the original primitive variable formulation has been replaced by a stream function-vorticity formulation, thereby eliminating previous numerical problems with regard to maintaining divergence-free flow.

INTRODUCTION

In Ref. 1 (hereafter denoted I) a two-dimensional, unsteady, finite difference, computer code "WAKE" was documented and used to investigate vortex interactions and turbulent transport in aircraft wakes. The thrust of I was to investigate the phenomenon of merging or coalescing of vortices in multivortex pair wakes. One major conclusion of this study was that vortex pairs can be made to interact in a favorable way so as to reduce the hazard induced on an encountering aircraft. After this interaction was complete, however, it was shown that the decay of the wake in the absence of atmospheric effects was a very slow process. The study contained herein is an extension of I and was undertaken to determine the effects of atmospheric turbulence, shear, and stratification as well as to investigate the dynamics of vortex interaction with the ground plane. In addition, general improvements were made to the "WAKE" code which reduced computational time with no sacrifice in accuracy. The study contained herein assumes that vortex interactions are complete, and that vortex merging has occurred and that the vortex wake can now be characterized by two counter-rotating vortices of circulation Γ, with separation b.

The fact that our atmosphere can be sheared, turbulent, and stably stratified simultaneously has made difficult the interpretation of vortex data obtained during flight tests. Apparently it is quite difficult to measure atmospheric parameters sufficiently to quantify the dissipative ability of the atmosphere, particularly since these measurements must not necessarily be made near the ground. For these reasons, it was decided to analytically investigate atmospheric effects by devising computational models which examined atmospheric turbulence, crosswind shear, and stratification separately. It is felt that this approach should both produce a maximum understanding as well as quantitative predictions of the dissipative ability of the atmosphere.

This report is organized as follows. In Section 2, changes made to the "WAKE" code are detailed including a description as to how a viscous ground plane has been augmented into the code. In Section 3, results are presented as to how atmospheric effects in a neutral atmosphere result in decay of a vortex pair. It is noted here that much of the material contained in Section 3 is included as an appendix and has been presented at the American Institute of Aeronautics and Astronautic's 16th Aerospace Sciences Meeting in Huntsville, Alabama. In Section 4, vortex descent in a stable atmosphere is investigated. In Section 5, results of several additional computations are presented which include roll up of a vortex sheet as well as computations of vortex ascent in an enclosed wind tunnel. Lastly, in Section 6, conclusions and recommendations are offered.

NOMENCLATURE

A, b, s, v_c	constants of the invariant second-order closure model
b	separation between vortices
C_ℓ	rolling moment coefficient, $\alpha \int_{-s_f}^{s_f} yW dy$
$D_{ind.}$	induced drag
Fr	Froude number, $\Gamma \left[-\rho_o/g \frac{d\rho}{dz}\right]^{\frac{1}{2}} \Big/ 2\pi s^2$
g_i	gravity (0,0,g)
H	stratification scale height
N	Brunt-Väisälä circular frequency, $\left[-\frac{g}{\rho_o}\frac{d\rho}{dz}\right]^{\frac{1}{2}}$
P	pressure
q	r.m.s. turbulence level
r	radial coordinate measured from vortex center
s	semi-separation between vortices $(2s = b)$
s_1, s_2, s_3, s_4	turbulent model constants of the scale equation
t	time
u, v, w	fluctuating velocity components in the x, y, z coordinate system
U, V, W	mean velocity components in the x, y, z coordinate system
U^*	friction velocity
x, y, z	Cartesian coordinates
$\bar{y}$	y centroid of vortex
$\bar{z}$	z centroid of vortex
z_o	surface roughness height
$\bar{z}_{max}$	maximum descent of vortex pair in a stably stratified atmosphere

β	departure of induced drag from that of elliptically loaded wing
Γ	circulation
γ	vortex sheet strength
η	streamwise component of vorticity
Θ	mean temperature
θ	fluctuating temperature
κ	von Karman constant, 0.37
Λ	macro or integral scale parameter
ν	kinematic viscosity
ρ	density
σ	Gaussian spread parameter
τ_g	Brunt-Väisälä period, $2\pi\left[-\rho_o/g \frac{d\rho}{dz}\right]^{\frac{1}{2}}$
ψ	stream function

Subscripts

f	follower
o	initial or reference

2. THE "WAKE" CODE

The "WAKE" code is a two-dimensional, unsteady, incompressible computer program developed to simulate the dynamics of multiple aircraft vortices in a turbulent stratified atmosphere. The two-dimensional approximation is justified for these flows since gradients in the flight x direction are very small compared with changes in the vertical z and lateral y directions. Therefore, a numerical simulation is equivalent to observing a wake flowfield in a plane which is both perpendicular to the aircraft's flight direction and fixed to the ground. Incompressibility is justified since the Mach number of the swirling velocities in the wake is small. The "WAKE" code is operational on the NASA Langley computers.

2.1 Equations of Motion

The continuity, momentum, and energy equations govern the solution to well-posed incompressible, turbulent, stratified flow problems which are of interest in the study of vortex wakes. Unfortunately, full numerical unsteady solution to these equations are beyond today's current computer hardware and software capabilities. To overcome this problem, turbulent transport in fluids is estimated with transport models which have been developed to be compatible with today's resources. The approach used here is to numerically solve for ensemble averaged mean field and ensemble averaged second-order correlations. The current model is one which has been used to predict successfully both quantitative and qualitative features of many turbulent flowfields (Refs. 1 - 4).

The model equations are briefly reviewed . Let each dependent variable be written as the sum of a mean and a fluctuating part (e.g., $U_i = U_i + u_i$) . After formal substitution into the continuity, momentum, and energy equations and ensemble averaging, the equations for the mean fields become;

Continuity

$$\frac{\partial U_i}{\partial x_i} = 0 \tag{2.1}$$

Momentum

$$\frac{DU_i}{Dt} = - \frac{\partial \overline{u_i u_j}}{\partial x_j} + \frac{\partial}{\partial x_j}\left(\nu \frac{\partial U_i}{\partial x_j}\right) - \frac{1}{\rho}\frac{\partial P}{\partial x_i} + \frac{g_i}{\Theta_o}(\Theta - \Theta_o) \tag{2.2}$$

Energy

$$\frac{D\Theta}{Dt} = - \frac{\partial \overline{u_i \theta}}{\partial x_i} + \frac{\partial}{\partial x_i} \left(\nu \frac{\partial \Theta}{\partial x_i} \right) \tag{2.3}$$

where

$$\frac{D}{Dt} = \frac{\partial}{\partial t} + U_j \frac{\partial}{\partial x_j}$$

We have assumed that the flow is incompressible but have permitted small changes in the density due to changes in temperature. The Boussinesq approximation has been used whereby the only effect of the density variation is in the body force term in the mean momentum equation.

In order to solve for the second-order correlation ensembled averages, $\overline{u_i u_j}$ and $\overline{u_i \theta}$, which are needed in the mean equations, the mean equations, Eq. (2.2) and Eq. (2.3), are subtracted from the complete equations. This operation leaves equations for u_i and θ which can be premultiplied and averaged to yield equations for $\overline{u_i u_j}$ and $\overline{u_i \theta}$. These equations are then closed by modeling third-order as well as certain second-order correlations. The details of this closure are not given here but are discussed in Ref. 5.

The modeled rate equations for the second-order correlations are as follows;

$$\begin{aligned} \frac{D}{Dt} \overline{u_i u_j} = & - \overline{u_i u_k} \frac{\partial U_j}{\partial x_k} - \overline{u_j u_k} \frac{\partial U_i}{\partial x_k} + \frac{g_i}{\theta_o} \overline{u_j \theta} + \frac{g_j}{\theta_o} \overline{u_i \theta} \\ & + v_c \frac{\partial}{\partial x_k} \left(q\Lambda \frac{\partial \overline{u_i u_j}}{\partial x_k} \right) - \frac{q}{\Lambda} \left(\overline{u_i u_j} - \delta_{ij} \frac{q^2}{3} \right) \\ & + \nu \frac{\partial^2 \overline{u_i u_j}}{\partial x_k^2} - \delta_{ij} \frac{2bq^3}{3\Lambda} \end{aligned} \tag{2.4}$$

$$\frac{D}{Dt}\,\overline{u_i\theta} = -\,\overline{u_iu_k}\,\frac{\partial\Theta}{\partial x_k} - \overline{u_k\theta}\,\frac{\partial U_i}{\partial x_k} + \frac{g_i}{\Theta_o}\,\overline{\theta^2}$$

$$+\,v_c\,\frac{\partial}{\partial x_k}\left(q\Lambda\,\frac{\partial\overline{u_i\theta}}{\partial x_k}\right) - \frac{Aq}{\Lambda}\,\overline{u_i\theta} + \nu\,\frac{\partial^2\overline{u_i\theta}}{\partial x_k^2} \qquad (2.5)$$

$$\frac{D\overline{\theta^2}}{Dt} = -\,2\overline{u_k\theta}\,\frac{\partial\Theta}{\partial x_k} + v_c\,\frac{\partial}{\partial x_k}\left(q\Lambda\,\frac{\partial\overline{\theta^2}}{\partial x_k}\right) + \nu\,\frac{\partial^2\overline{\theta^2}}{\partial x_k^2} - \frac{2bsq\overline{\theta^2}}{\Lambda} \qquad (2.6)$$

where $q^2 = \overline{u_iu_i}$ (the summation convention is implied) and Λ is a measure of the macroscale of the turbulence. The constants v_c, b, A and s are constants of the invariant second-order closure model. They are assigned the values 0.3, 0.125, 0.75 and 1.8, respectively. These values have been chosen from computer simulations of turbulent flows where experimental data are available (see Ref. 5 for a complete description). The scale Λ is a measure of the large eddies to be found in a flow. The scale is, therefore, itself determined from a differential scale equation

$$\frac{D\Lambda}{Dt} = -\,s_1\,\frac{\Lambda}{q^2}\,\overline{u_iu_k}\,\frac{\partial U_i}{\partial x_k} - s_2q + v_c\,\frac{\partial}{\partial x_k}\left(q\Lambda\,\frac{\partial\Lambda}{\partial x_k}\right)$$

$$-\,\frac{s_3}{q}\left(\frac{\partial q\Lambda}{\partial x_k}\right)^2 + s_4\,\frac{\Lambda}{q^2}\,\frac{g_i}{\Theta_o}\,\overline{u_i\theta} \qquad (2.7)$$

where the constants s_1, s_2, s_3, and s_4 have the values -0.35, -0.6, 0.375, and 0.8. Equations (2.1) through (2.7) are the second-order invariant model of turbulent transport.

2.2 Superequilibrium

The above turbulent transport model has a simple limit which is useful analytically to fix background turbulent atmospheres through which vortices will be allowed to descend. This limit exists when second-order correlations have equilibrated to the mean field; hence the name superequilibrium is used. The superequilibrium limit of the turbulent model is found by neglecting convection and diffusion terms in the equations for the second-order correlations.

In addition, the high Reynolds number limit of the dissipation terms is taken. The resulting equations for the turbulent correlations are

$$0 = -\ 2\overline{uw}\,\frac{\partial U}{\partial z} - \frac{q}{\Lambda}\,\overline{uu} + (1 - 2b)\,\frac{q^3}{3\Lambda} \tag{2.8}$$

$$0 = -\ \frac{q}{\Lambda}\,\overline{vv} + (1 - 2b)\,\frac{q^3}{3\Lambda} \tag{2.9}$$

$$0 = \frac{2g}{\Theta_o}\,\overline{w\theta} - \frac{q}{\Lambda}\,\overline{ww} + (1 - 2b)\,\frac{q^3}{3\Lambda} \tag{2.10}$$

$$0 = -\ \overline{ww}\,\frac{\partial U}{\partial z} + \frac{g}{\Theta_o}\,\overline{u\theta} - \frac{q}{\Lambda}\,\overline{uw} \tag{2.11}$$

$$0 = -\ \overline{uw}\,\frac{\partial \Theta}{\partial z} - \overline{w\theta}\,\frac{\partial U}{\partial z} - \frac{A\overline{u\theta}q}{\Lambda} \tag{2.12}$$

$$0 = -\ \overline{ww}\,\frac{\partial \Theta}{\partial z} + \frac{g}{\Theta_o}\,\overline{\theta^2} - \frac{A\overline{w\theta}q}{\Lambda} \tag{2.13}$$

$$0 = -\ 2\overline{w\theta}\,\frac{\partial \Theta}{\partial z} - 2bs\,\frac{q\overline{\theta^2}}{\Lambda} \tag{2.14}$$

where it has been assumed that $U_i = [U(z),0,0]$ and that $\Theta = \Theta(z)$. The solution of Eq. (2.8) through Eq. (2.14) may be computed if the following definitions are introduced.

$$\overline{uu} = UU\Lambda^2\left(\frac{\partial U}{\partial z}\right)^2 \qquad \overline{u\theta} = UT\Lambda^2\left(\frac{\partial U}{\partial z}\right)\left(\frac{\partial \Theta}{\partial z}\right)$$

$$\overline{vv} = VV\Lambda^2\left(\frac{\partial U}{\partial z}\right)^2 \qquad \overline{w\theta} = WT\Lambda^2\left(\frac{\partial U}{\partial z}\right)\left(\frac{\partial \Theta}{\partial z}\right)$$

$$\overline{ww} = WW\Lambda^2\left(\frac{\partial U}{\partial z}\right)^2 \qquad \overline{\theta^2} = TT\Lambda^2\left(\frac{\partial \Theta}{\partial z}\right)^2$$

$$\overline{uw} = UW\Lambda^2\left(\frac{\partial U}{\partial z}\right)^2 \qquad q^2 = QQ\Lambda^2\left(\frac{\partial U}{\partial z}\right)^2 \tag{2.15}$$

and note that

$$QQ = Q^2 = UU + VV + WW \tag{2.16}$$

Substitution of the definitions, Eq. (2.15) and Eq. (2.16) into Eq. (2.8) through Eq. (2.14) results in a system of nonlinear algebraic equations which may be solved to give expressions for the turbulent correlations in terms of the stratification $\partial\Theta/\partial z$, the shear $\partial U/\partial z$, and the scale Λ. A discussion of the stabilizing effects of stratification and rotation in the superequilibrium limit is given in Refs. 6-8.

2.3 Solution Algorithm

The solution algorithm is the same as that described in I with one significant change; the mean equations have been solved in terms of stream function-vorticity variables. Note that Eq. (2.1) in the two-dimensional approximation is

$$\frac{\partial V}{\partial y} + \frac{\partial W}{\partial z} = 0 \tag{2.17}$$

which allows the definition of a stream function ψ :

$$V = \frac{\partial \psi}{\partial z} \quad , \quad W = - \frac{\partial \psi}{\partial y}$$

Then the x component of vorticity η is

$$\eta = \frac{\partial W}{\partial y} - \frac{\partial V}{\partial z} \tag{2.18}$$

such that the stream function satisfies a Poisson equation

$$\frac{\partial^2 \psi}{\partial y^2} + \frac{\partial^2 \psi}{\partial z^2} = - \eta \tag{2.19}$$

Equations (2.2) with $i = 2,3$ are then cross differentiated and subtracted to eliminate pressure to yield a transport equation for the streamwise component of vorticity

$$\frac{D}{Dt}\eta = \nu\nabla^2\eta - \frac{\partial^2}{\partial y^2}\overline{vw} + \frac{\partial^2}{\partial z^2}\overline{vw} - \frac{\partial^2}{\partial y \partial z}(\overline{ww} - \overline{vv}) + \frac{g}{\Theta_o}\frac{\partial\Theta}{\partial y} \tag{2.20}$$

The resulting system of equations finally consists of the mean vorticity equation, Eq. (2.20), and Eq. (2.3) through Eq. (2.7). The Poisson equation, Eq. (2.19), is then solved for ψ using a fast direct solver developed by Swartztrauber and Sweet (Ref. 9). The velocity field may then be computed from the definition of the stream function. Use of the stream function-vorticity system eliminates the need to compute the pressure field and automatically insures that continuity, Eq. (2.17), is satisfied, as opposed to the algorithm employed in I where a correction for continuity must be added at each time step. In addition, boundary conditions for the stream function (needed for solving the Poisson equation) may be directly related to the velocity components V and W, while the choice of boundary conditions for pressure in I is less clear.

2.4 Boundary Conditions

The "WAKE" code is designed to accept boundary conditions of the form $Ae + B(\partial e/\partial n) + C = 0$ on the variable e on any of the four sides of the computational domain. A, B, C may be functions of y, z, t and $\partial/\partial n$ is the normal derivative. Two special cases of the above are described below.

Rigid Wall - Law of the Wall

Vortices descending in ground effect must experience a de-intensification as a result of viscous scrubbing along the ground. In order to quantify the amount of dissipation which results, a viscous no slip boundary condition is needed. Instead of resolving the wall boundary layer with a finite difference mesh, it is more efficient to develop an asymptotic wall layer condition. This is accomplished by noting that asymptotically the velocity shear in the neighborhood of a wall (say at $z = 0$) of surface roughness z_o, is given by

$$\frac{\partial V}{\partial z} = \frac{U^*}{\kappa} \frac{1}{z} \tag{2.21}$$

where U^* is a to be determined friction velocity and κ is von Karman's constant. In this wall layer, since $(\partial/\partial z) >> (\partial/\partial y)$, Eq. (2.21) defines an approximation to the vorticity, i.e.,

$$\eta \simeq - \frac{\partial V}{\partial z} = - \frac{U^*}{\kappa} \frac{1}{z} \tag{2.22}$$

Integration of Eq. (2.22) yields

$$V = \frac{\partial \psi}{\partial z} = \frac{U^*}{\kappa} \log \frac{z}{z_o} \tag{2.23}$$

and

$$\psi = \frac{U^*}{\kappa} \left[z \log \frac{z}{z_o} - (z - z_o) \right] \tag{2.24}$$

These expressions are obtained by requiring that $\psi = \psi_z = 0$ at $z = z_o$.

The finite difference grid will not adequately resolve the dependent quantities in the steep turbulent boundary layer region. We will instead use the expressions, Eq. (2.22) - Eq. (2.24), to define a boundary condition at a reference level z_r above the wall, but within the asymptotic region where these equations are valid. The reference level z_r is the first mesh point in the computational domain. To define boundary conditions, consider the finite difference formulation for η and V in terms of ψ :

$$\eta_r = \frac{-\psi_{r+1} + 2\psi_r - \psi_{r-1}}{(\Delta z)^2} \tag{2.25}$$

$$V_r = \frac{\psi_{r+1} - \psi_{r-1}}{2\Delta z} \tag{2.26}$$

where Δz is the mesh size and ψ_r represents the streamfunction at z_r and $\psi_{r\pm 1}$ is the streamfunction at the mesh points above and below z_r (z_{r-1} is a fictitious point). Equation (2.26) can also be written as

$$\frac{\psi_{r+1} - \psi_{r-1}}{2\Delta z} \simeq V_r = \frac{U^*}{\kappa} \log \frac{z_r}{z_o}$$

or

$$\frac{\psi_{r+1} - \psi_{r-1}}{2\Delta z} = - \eta z \log \frac{z}{z_o} \tag{2.27}$$

Elimination of ψ_{r-1} from Eq. (2.25) and Eq. (2.27) yields

$$\eta_r = \frac{- 2(\psi_{r+1} - \psi_r)}{\left(1 + 2 \frac{z}{\Delta z} \log \frac{z}{z_o}\right) (\Delta z)^2} \tag{2.28}$$

the boundary condition for η in terms of ψ . Eliminating U^* from Eq. (2.22) and Eq. (2.24) yields

$$\psi_r = - \eta_r[z \log \frac{z}{z_o} - (z - z_o)]z , \tag{2.29}$$

the boundary condition on ψ .

Radiation or Advection Conditions

Vortices descending into a stably stratified fluid will generate internal waves which will propagate to the edges of the computational domain. If upon reaching the boundary, some condition is not employed to allow these waves to pass out of the domain, they will be reflected back and possibly spoil the computation. No one universal technique has been devised to avoid this problem. Specification of boundary conditions on a finite computational domain representing an infinitely large stratified domain is both challenging andfrustrating, requiring both physical insight and art. Previously, one technique which we have employed was to apply a porous liner near the computational boundaries. This is accomplished by adding damping terms to the equations of motion, the strength of the damping increasing as the boundary is approached (Ref. 9). This technique has been abandoned since it is difficult to accurately assess how much artifical damping is actually added to the computation. Modest success has been achieved with the use of a Sommerfield radiation condition which is described below.

Boundary conditionsof the type

$$\frac{\partial e}{\partial t} + c\,\frac{\partial e}{\partial n} = 0 \tag{2.30}$$

propagate the quantity e at velocity c in the n direction. If c is the phase speed of internal waves as they approach the boundary, Eq. (2.30) should allow these waves to propagate out of the domain. The success of this condition rests with the accurate specification of c and with a narrow width of the wave number spectrum which must be passed out of the domain.

If c is a fluid speed, Eq. (2.30) is an advection condition. For example, in the case of a pair of descending vortices, a downward moving coordinate system can be imposed which will keep the vortices of interest in the center of the domain. This means that fluid will be washing out through the top of the domain. A suitable condition for the top boundary would be to set c equal to the local vertical velocity when e is a variable which will be advected out, e.g., the vorticity.

3. VORTEX DECAY IN NEUTRAL ATMOSPHERES VORTEX/GROUND PLANE INTERACTION

The investigation of atmospheric effects as they influence the decay of aircraft wake vortices can be separated as to whether the atmosphere is neutral or stably stratified. In this section, results obtained for descent of aircraft vortices in a neutral atmosphere are summarized. Details of the work undertaken may be found in the Appendix which is a preprint of the work entitled, "The Role of Atmospheric Shear, Turbulence and a Ground Plane on the Dissipation of Aircraft Vortex Wakes." This work was presented at the 16th Aerospace Sciences Meeting in Huntsville, Alabama. Results of three types of computations are presented and discussed. They are;

1. Computations undertaken to evaluate the effectiveness of background ambient turbulence on the dissipation of a vortex wake.

2. Computations undertaken to evaluate the effectiveness of crosswind shear on the dissipation of a vortex wake.

3. Computations undertaken to evaluate the effectiveness of the ground on the dissipation of a vortex wake.

The following conclusions have been drawn;

Vortex pairs in a turbulent background - Numerical computations have shown that the decay of a vortex pair in a turbulent atmosphere is greatly enhanced by the presence of turbulence. Direct computation has shown that the decay of circulation in a square contour positioned on the vortex "center" decays as t^{-2} when turbulence is present. This is compared to a computed $t^{-1/2}$ decay when the ambient turbulence is zero and the pair diffuses as a result of its own internally generated turbulence. Computations have shown that turbulence levels typical of the atmosphere can reduce the circulation by a factor of three or so one minute after passage of a B747 aircraft. The inability to directly correlate real data with computations is tied to failure to quantify the scale of turbulence in the atmosphere. Work is currently under way to validate models which predict integral scale lengths.

Vortex pairs in a crosswind shear - During flight tests, vortices are marked with smoke for visualization purposes. Under certain conditions the smoke in one vortex would vanish, leaving what appeared to be a solitary vortex (Ref.10). It was conjectured at the time of observation that the solitary vortex may pose a more serious problem than a pair wake and that the phenomenon was in some way brought about by atmospheric shear. Computations run with crosswind shear essentially confirm that shear disperses the vortex whose vorticity is of the opposite sign of the vorticity associated with the shear. However, direct computations cannot confirm that the remaining vortex will be a more significant hazard than a comparable pair wake. Basically, the decay of the solitary vortex is strongly influenced by the turbulence associated with the cross shear. It has been speculated, that over tens of minutes it is possible to have shear without turbulence and turbulence without shear when the atmosphere is stably stratified. Under these conditions, it may indeed be possible to have a solitary vortex which may persist for a long period of time.

Vortex ground plane interaction - Vortices in close proximity to the ground must feel some decay of strength as a consequence of scrubbing of fluid along the ground. To quantify this effect computations were run with a viscous turbulent law of the wall boundary condition applied at ground level. The results of these computations were quite surprising in that the vortices did not follow the classical hyperbolic trajectories but rebounded from the ground plane. This rebounding or bouncing phenomenon results from secondary vorticity generated at the ground being swept up and convected about the primary vortices. This result is significant in that it provides a mechanism by which vorticity of opposite sign can be mixed with the vortex wake and thereby augment the decay process. Direct computation suggests that rolling moment induced on a follower aircraft may be reduced by a factor of 3 after one minute of the passage of a B747 aircraft.

4. STABLE ATMOSPHERIC STRATIFICATION

In this section the descent of a vortex pair in a stably stratified, incompressible atmosphere is investigated. This study is the first which includes turbulent transport directly. Motivation has come from the several previously published analytical investigations, (Refs. 11-15); most of which are in disagreement. This disagreement, as discussed by Widnall (Ref. 16), results from the different accounting of fluid impulse and energy and the entraining/detraining of mass and vorticity from the interface of the descending oval of fluid. The computations discussed below will suggest that the dynamics of the descent of a vortex pair in a stably stratified flow is intimately tied to the correct accounting of turbulent transport effects.

4.1 Physical Effects of Stratification

Consider a linearly stratified stable incompressible fluid with the unperturbed density given by

$$\rho = \rho_o + \frac{d\rho}{dz} z \tag{4.1}$$

The characteristic scale height H of the stratification is defined

$$H = \rho_o \Big/ \frac{d\rho}{dz} \tag{4.2}$$

and is assumed to be much greater than the characteristic vortex spacing b . The characteristic time of a gravity wave is known to be

$$\tau_g = \left[-\rho_o \Big/ g \frac{d\rho}{dz} \right]^{1/2} \tag{4.3}$$

A measure of the importance of stratification is to compare the characteristic vortex pair time $\tau_v = 2\pi s^2/\Gamma$ with the B.V. period. This ratio of time scales defines a Froude number which is

$$Fr = \frac{\Gamma}{2\pi s^2} \left[-\rho_o \Big/ g \frac{d\rho}{dz} \right]^{1/2} \tag{4.4}$$

The Froude number for a standard atmosphere at an altitude of 300 m can be computed to be of the order of 10 for a B747 aircraft. This implies that stratification effects are weak. An alternate interpretation is that the effects of stratification are significant after the vortex pair has descended; say five spans. The Froude number is infinite when the flow is neutrally stratified.

It is appropriate here to discuss qualitatively the anticipated effects of stratification prior to presenting numerical results. In Fig. 4.1(a) is shown the streamline pattern of a vortex pair descending in a neutral fluid. As is well known the vortex pair transports mass downward. This mass is that contained in the oval of recirculating fluid which is observed in a coordinate system moving with the vortex pair. As is also well known, this descent velocity is approximately $\Gamma/4\pi s$. In the absence of three-dimensional instability and ambient atmospheric turbulence, a vortex pair propagates with little change in velocity (see Fig. 2 in the Appendix). If this oval of fluid of density ρ_o were to descend into a fluid of density ρ_1 such that $\rho_1 > \rho_o$ it is anticipated that the behavior of the pair is significantly altered as a result of the vorticity which will be generated at the density discontinuity.

The origin of this vorticity can be seen by examining Eq. (2.20), where density ρ may be substituted for temperature Θ , since $\rho/\rho_o = - \Theta/\Theta_o$. The production term is

$$\frac{g}{\Theta_o} \frac{\partial \Theta}{\partial y} = -\frac{g}{\rho_o} \frac{\partial \rho}{\partial y} \tag{4.5}$$

and is proportional to the gradient of the density in the horizontal, y , direction. This density gradient is large at the oval interface.

It should be anticipated that the additional vorticity generated will alter the descent of the pair as a consequence of inducing an additional component of velocity on the descending vortices. We have schematically illustrated in Fig. 4.1 three possibilities. The centroids of the buoyancy generated vorticity are above the pair, below the pair or at the altitude of the pair. The first-order consequence of these centroid locations in the absence of turbulent diffusion would be to decrease the separation between vortices in the pair and possibly lead to an acceleration (Ref. 14), increase the separation or hold constant the separation, respectively. Unfortunately, turbulent diffusion alters this simple description.

4.2 Descent of a Vortex Pair in a Stably Stratified Atmosphere.

In order to study the decay of vortex pairs in a stably stratified atmosphere, simulations were run at three different Froude numbers with three levels of background turbulence (determined from superequilibrium theory), nine cases in all.

The computations are initialized by positioning a Gaussian of vorticity of the form $\eta 2\pi s^2/\Gamma = \pm(2/\sigma^2) \exp[-(r/s)^2/\sigma^2)]$ at $y/s = \pm 1$; $z/s = 0$, respectively. The coordinate r is measured radially from the vortex center and σ is the vortex spread ($\sigma = 0.5$ for all computations). The numerical mesh is specified for only $y > 0$ since symmetries about $y = 0$ can be utilized. In addition to the uniform level of background turbulence, an isotropic Gaussian spot

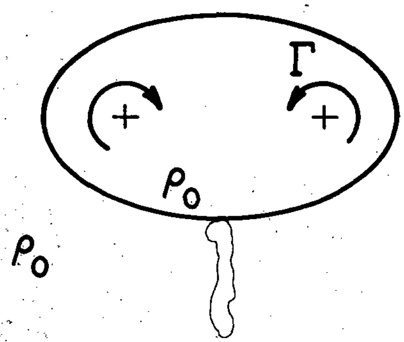

(a) The descent of a vortex pair in a neutral fluid

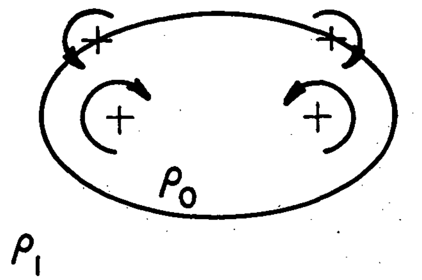

(b) Vorticity generated at density discontinuity tends to reduce vortex pair separation

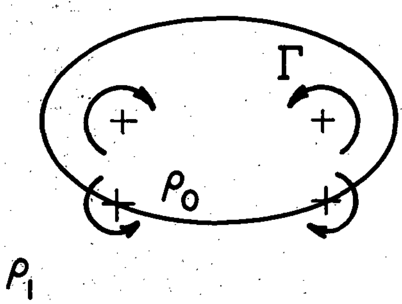

(c) Vorticity generated at density discontinuity tends to increase vortex pair separation

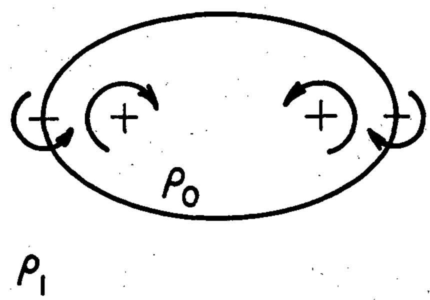

(d) Vorticity generated at density discontinuity tends to keep vortex pair separation constant

Figure 4.1. Postulated behaviors of a vortex pair in a buoyant inviscid fluid

of turbulence is positioned in the center of each vortex of strength $(q_o 2\pi s/\Gamma)^2 = 0.01$, such that $\langle uu \rangle = \langle vv \rangle = \langle ww \rangle = (q_o^2/3) \exp[-(r/s)^2/\sigma^2)]$. A passive tracer of the same Gaussian character with strength $C_o = 1$ is also positioned over the vortex centers. The background constant density gradient $[Fr\ 2\pi s^2/\Gamma]^2 (g/\rho_o)\ \partial\rho/\partial z = -1$ and the background axial velocity field is chosen such that the shear $(2\pi s^2/\Gamma)\ \partial U/\partial z$ is that required to give the proper level of background turbulence in accordance with superequilibrium theory. An upwash velocity is added to the solution in order to keep the vorticity in the center of the computational domain. This is equivalent to viewing the solution in a coordinate system that moves with the vortices. This upwash velocity is computed throughout the calculation such that the centroid of the passive tracer is kept in the center of the domain. The initial conditions are shown schematically in Fig. 4.2.

The boundary conditions are given in terms of the moving coordinate system. The stream function is computed from a Biot-Savart law as described in I with the addition of a contribution due to the moving coordinate system. The vorticity, density, and axial velocity are specified at the bottom of the domain by their values in the undisturbed fluid; namely, vorticity is zero and the density and axial velocity are determined by the background gradients that were specified initially. These three quantities are advected out through the top of the domain with the local vertical velocity as the domain descends into heavier fluid. At the outer edge of the domain, the condition on these quantities is that $\partial/\partial y = 0$. At the edges of the computational domain, except at the $y = 0$ boundary, turbulent quantities are assumed to have zero slope and the passive tracer is assumed to have zero value. The zero slope condition at the outer edge in the y direction is quite adequate at this boundary despite the presence of Brunt-Väisälä waves since the computations were not carried so far in time that a reflecting wave became a problem.

Nine cases were run with three different Froude numbers and three different values of initial background turbulence levels. These runs are summarized in Table 1 below.

All cases were run with a Reynolds number of 10^5 and a fixed value of the integral scale $\Lambda/s = 0.1$. Results of cases 4, 5, and 6 (no initial background turbulence) are shown in Figs. 4.3 and 4.4 Figure 4.3 is a plot of the descent velocity of the vortex measured by tracking the centroid of the smoke, while Fig. 4.4 is a plot of the penetration depth of the vortices as a function of time. Simulations were carried out until the descent velocity dropped to less than 0.1 from an initial value of 0.5. Note the much larger stopping times, as expected, for the higher Froude number (lower stratification) cases. It should be noted that the descent velocity is a monotonically decreasing function throughout the computation.

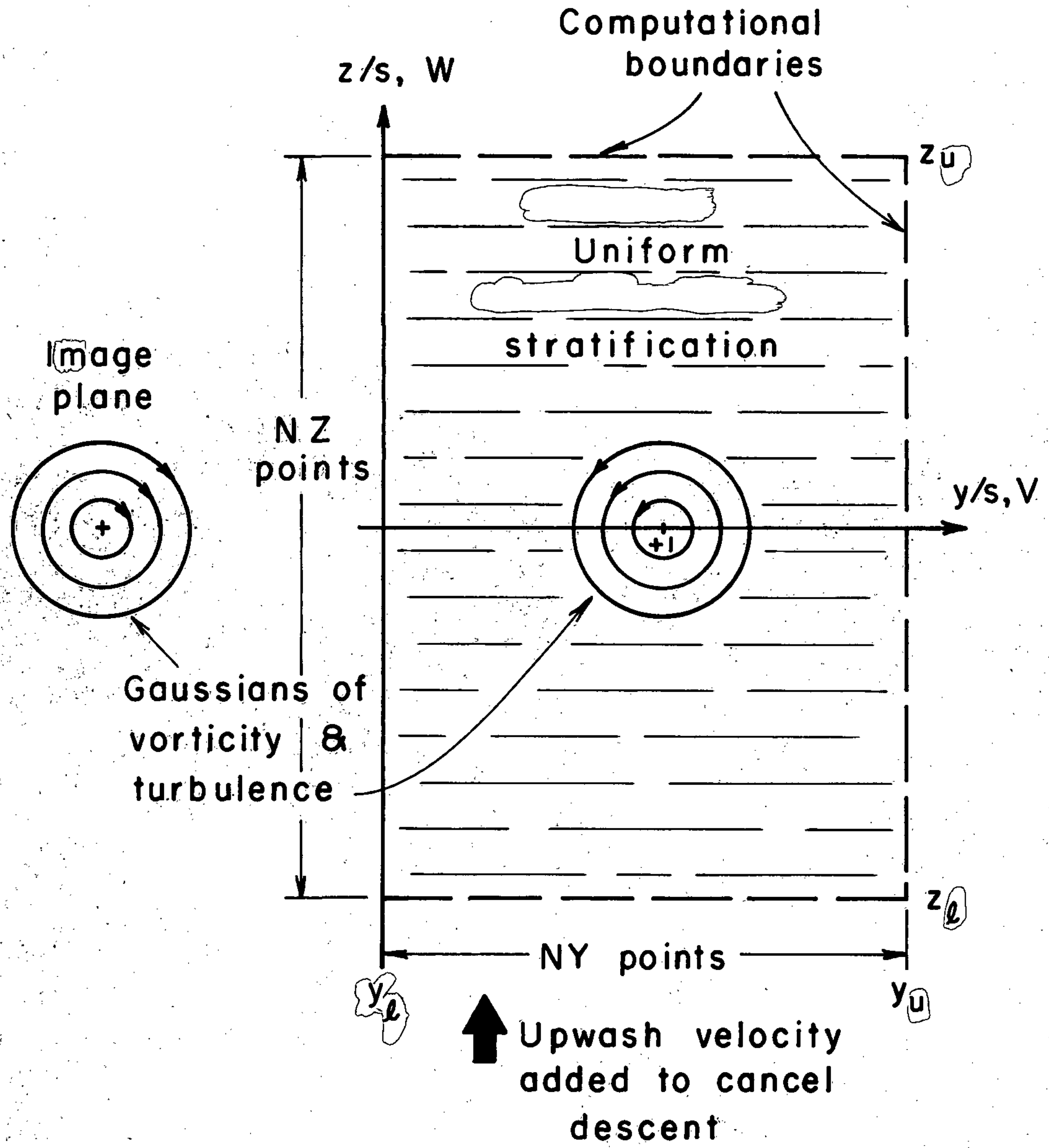

Figure 4.2. Schematic of initial conditions for the computation of a vortex pair descending in a stably stratified fluid.

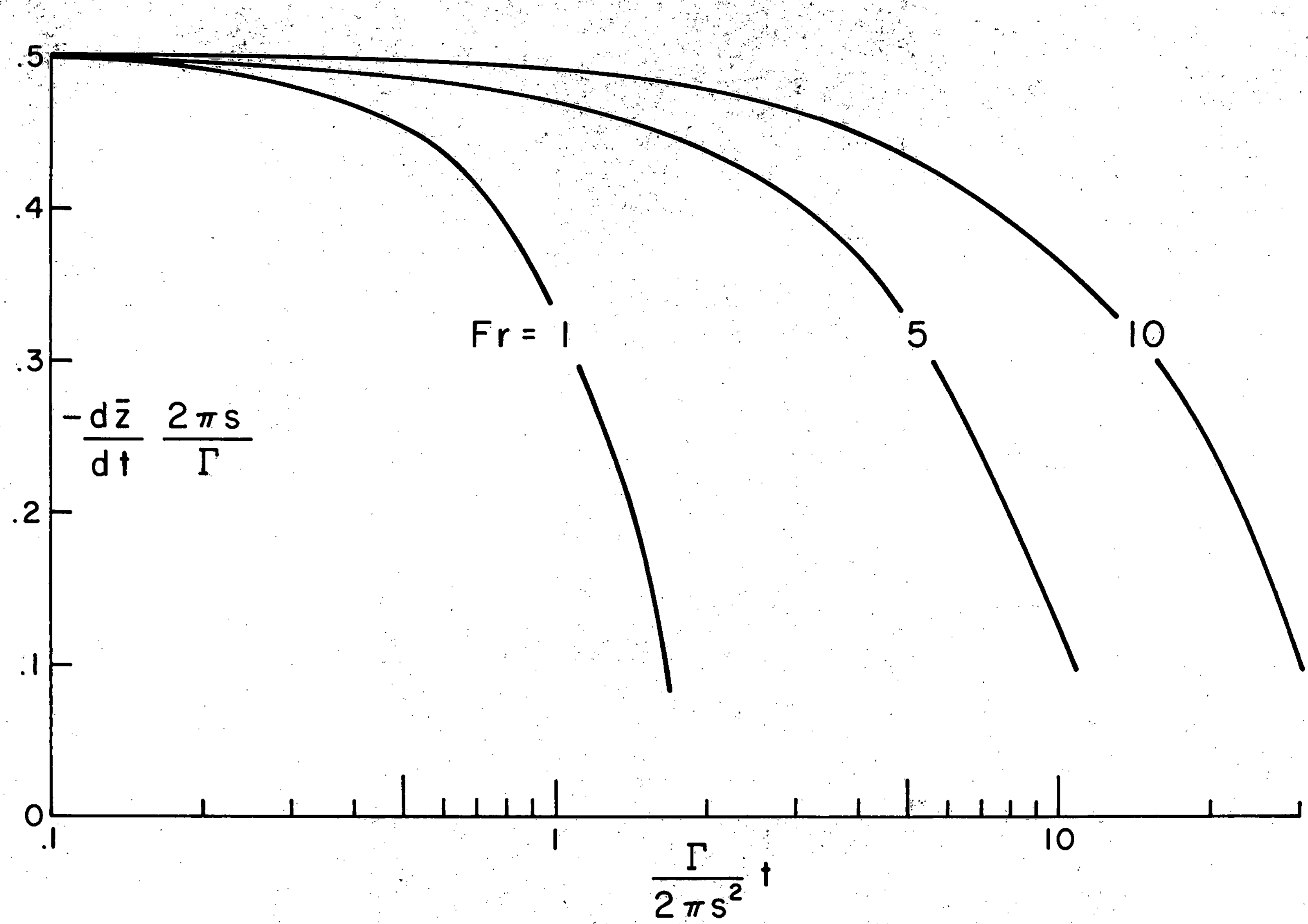

Figure 4.3. Descent velocity of the vortex pair versus time for cases 4, 5, and 6 with Froude numbers 1, 5, and 10.

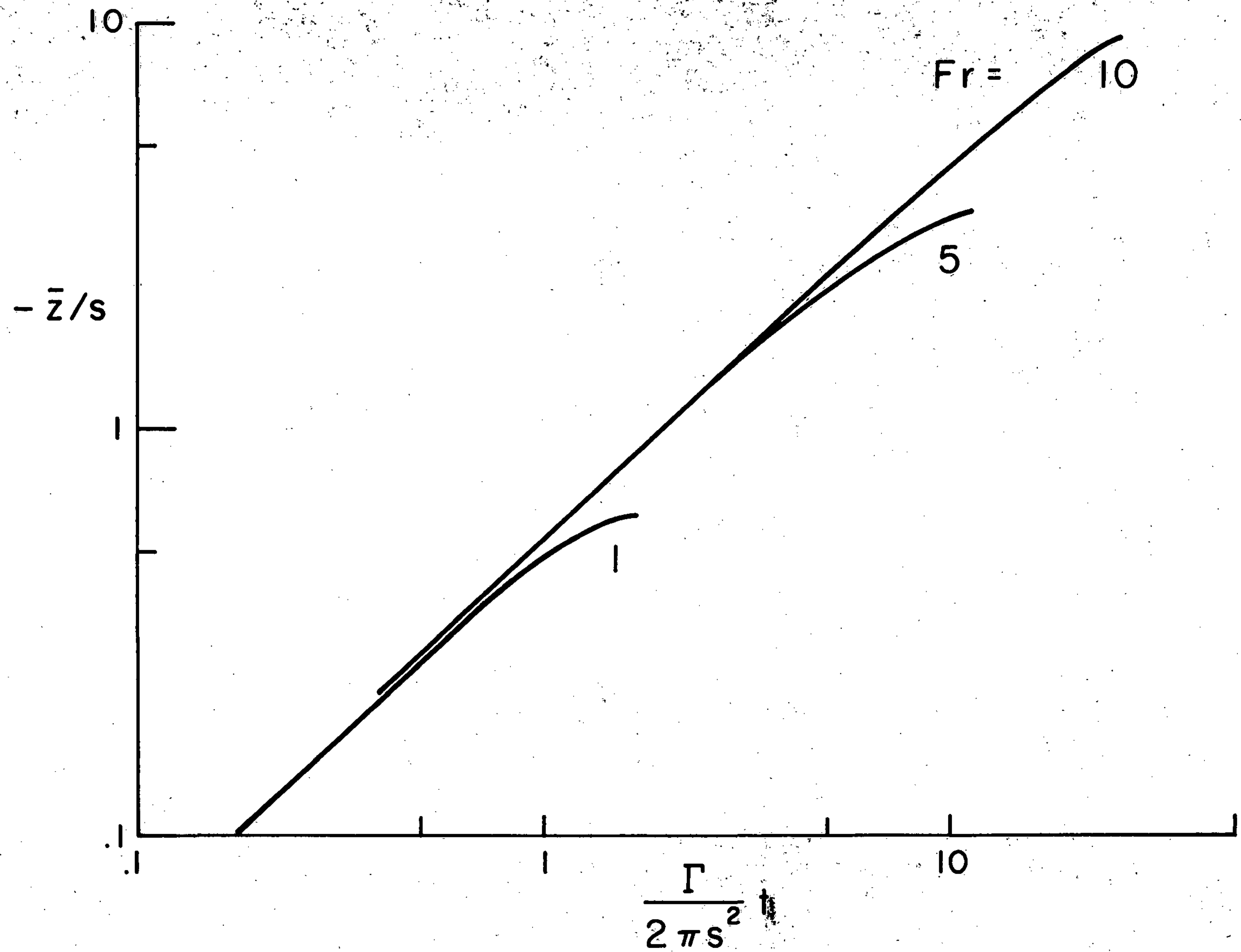

Figure 4.4. Penetration depth versus time for cases 4, 5, and 6 with Froude numbers 1, 5, and 10.

TABLE 1.

DESCENT OF A VORTEX PAIR INTO STABLE STRATIFICATION

Run	Fr	$(2\pi s/\Gamma)^2 q^2$	$(2\pi s/\Gamma)/(\partial U/\partial z)$
1	1.0	0.0090	1.43
2	5.0	0.0096	0.50
3	10.0	0.0091	0.39
4	1.0	0.0	0.0
5	5.0	0.0	0.0
6	10.0	0.0	0.0
7	1.0	0.00098	1.355
8	5.0	0.00094	0.310
9	1.0	0.00091	0.195

For case 6, NY = 32 , NZ = 45 , $z_\ell = -4.4$, $z_u = 4.4$, and $y_u = 7.0$. The grid in the z direction is uniform and the grid in the y direction is stretched to give maximum resolution near $y = 0$. For all other cases; NY = 33 , NZ = 40 , $z_\ell = -3.0$, $z_u = 5.0$, and $y_u = 3.2$ with uniform grids in both directions. (Refer to Fig. 4.2 for grid and domain size definitions.)

No acceleration of the pair is predicted.

Results of cases 1, 2, 3, 7, 8, and 9 where background turbulence levels are specified are not shown since they are nearly identical to the respective Froude number cases. This observation at first appears contradictory, but is simply explained by examining the maximum computed level of turbulence present in the vortex pair as a function of time. As can be seen in Fig. 4.5, the internally produced turbulence in the descending oval far exceeds the ambient value and, therefore, it is this internal process which intimately controls the descent of the pair in a stably stratified fluid.

In order to measure the decay rate of the vortices, rolling moments induced on a follower aircraft of wing semispan s_f have been computed and displayed in Fig. 4.6. It can be seen that the vortices have stopped their descent long before there has been any significant decay of rolling moment on the follower aircraft. This is a major finding in that vortices may, as a result of stable stratification, be observed to stop descending but may still be capable of inducing large rolling moments on an encountering aircraft.

4.3 A Simple Estimate of the Penetration of a Vortex Pair into a Stably Stratified Fluid.

Analysis of the streamline pattern generated while undertaking the above computations has shown that the volume of fluid descending is "approximately" constant during much of the descent. This can be seen in Figs. 4.7 and 4.8 where streamline patterns are shown for the $Fr = 1$ and 10 case, respectively. During the final stages of descent, when the descent velocity is approximately 25% of the initial value, recirculating oval sizes do change but the additional penetration distance covered after this time is small when compared to the total penetration. This observation suggests a simple model which can be used to estimate maximum penetration. This model is based on an energy balance.

The initial kinetic energy of the pair is related to the induced drag of the wing. Expressing the induced drag as a multiple of the drag of an elliptically loaded wing we write

$$D_{ind.} = \frac{\pi}{8}\beta\rho_o\Gamma_o^2 \qquad (4.6)$$

where β is a function of the spread of vorticity σ. For the sample computations above, β was numerically determined to be equal to 0.547. The final potential energy of an oval of area A, carrying fluid with density equal to that at its initial height, is given by

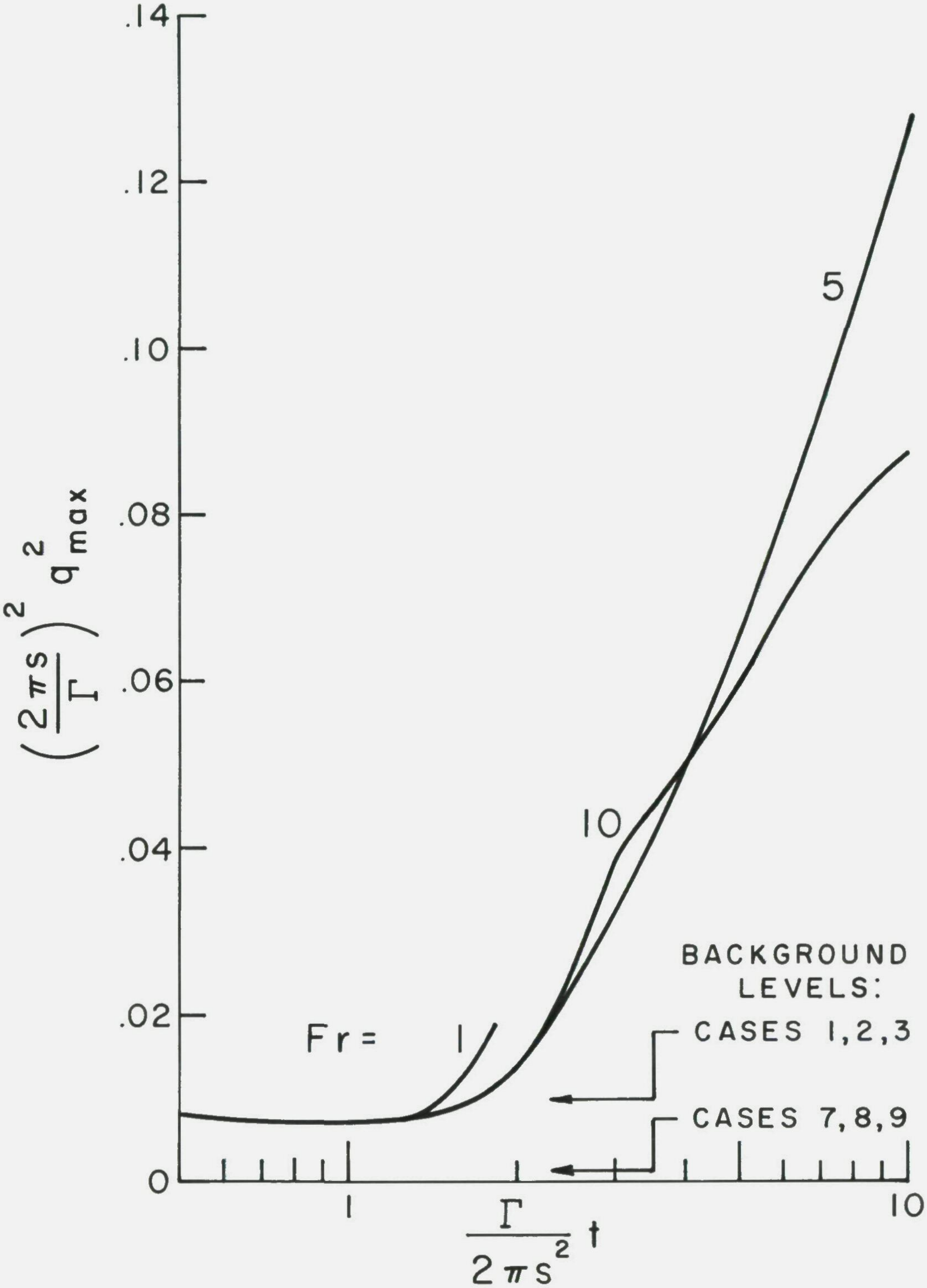

Figure 4.5. Maximum internally produced turbulence levels as a function of time for cases 4, 5, and 6 (background turbulence level = 0).

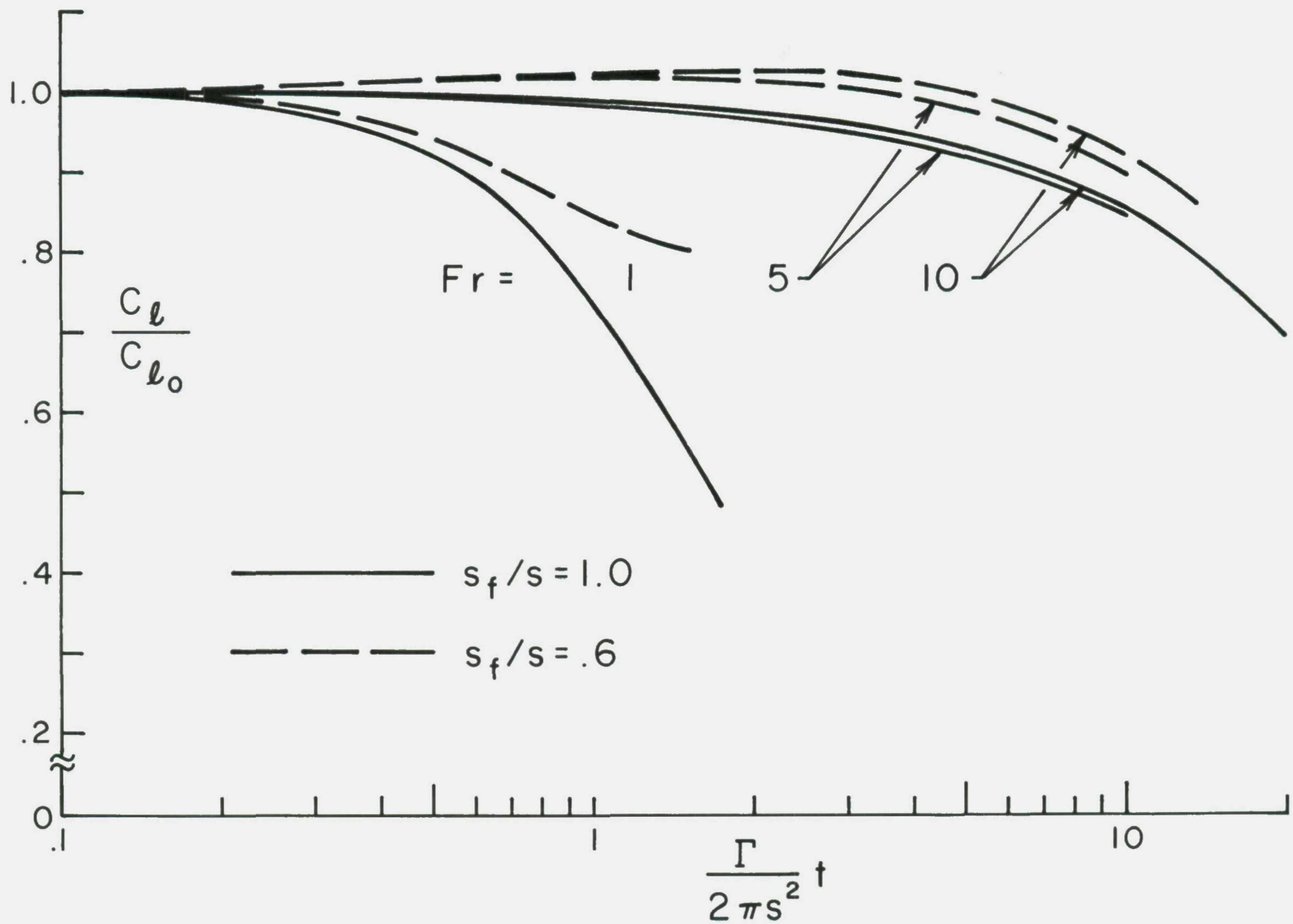

Figure 4.6. Rolling moment drop off as a function of time for follower aircraft of semispan s_f . Cases 4, 5 and 6.

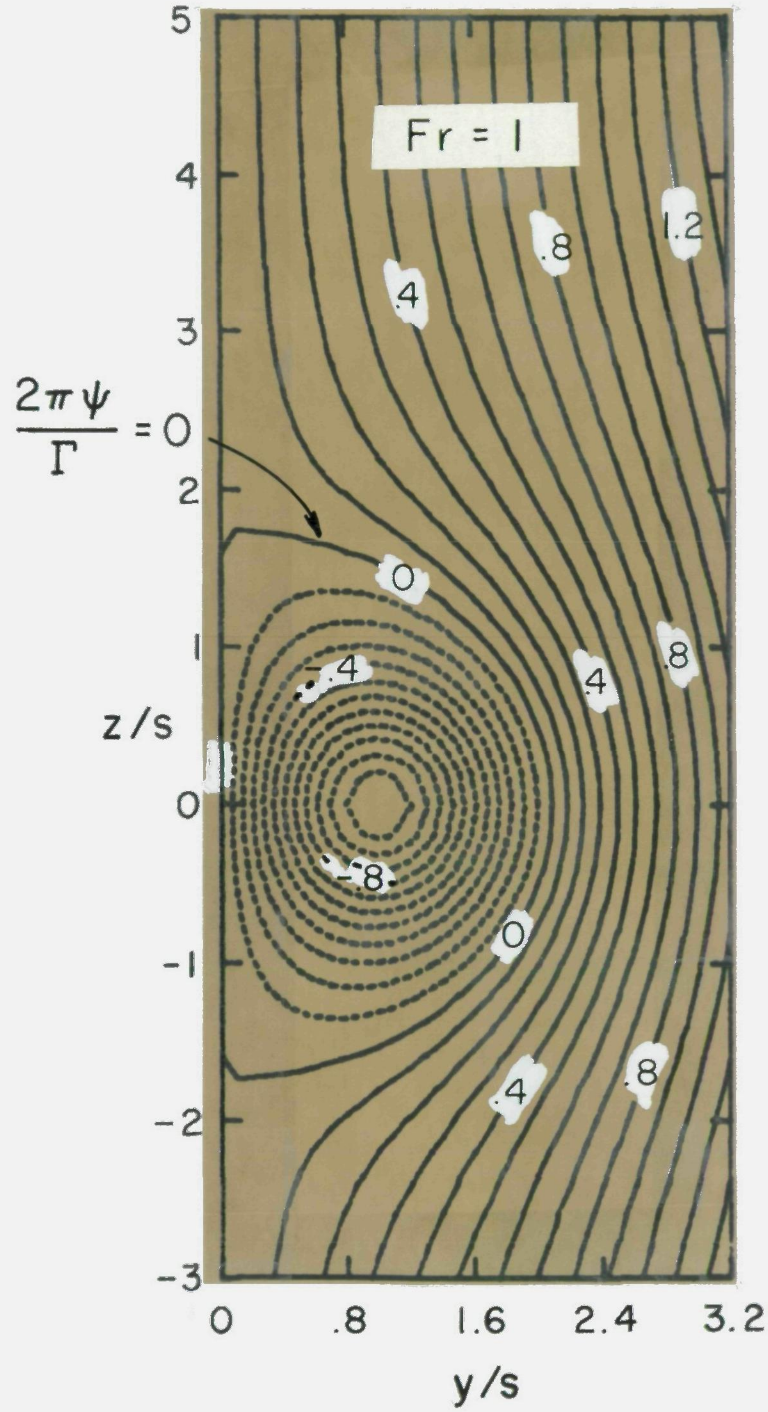

Figure 4.7 (a). Streamline pattern at $t\Gamma/2\pi s^2 = 0$, contour interval = 0.1 , descent velocity $-\frac{d\bar{z}}{dt}\frac{2\pi s}{\Gamma} = 0.5$.

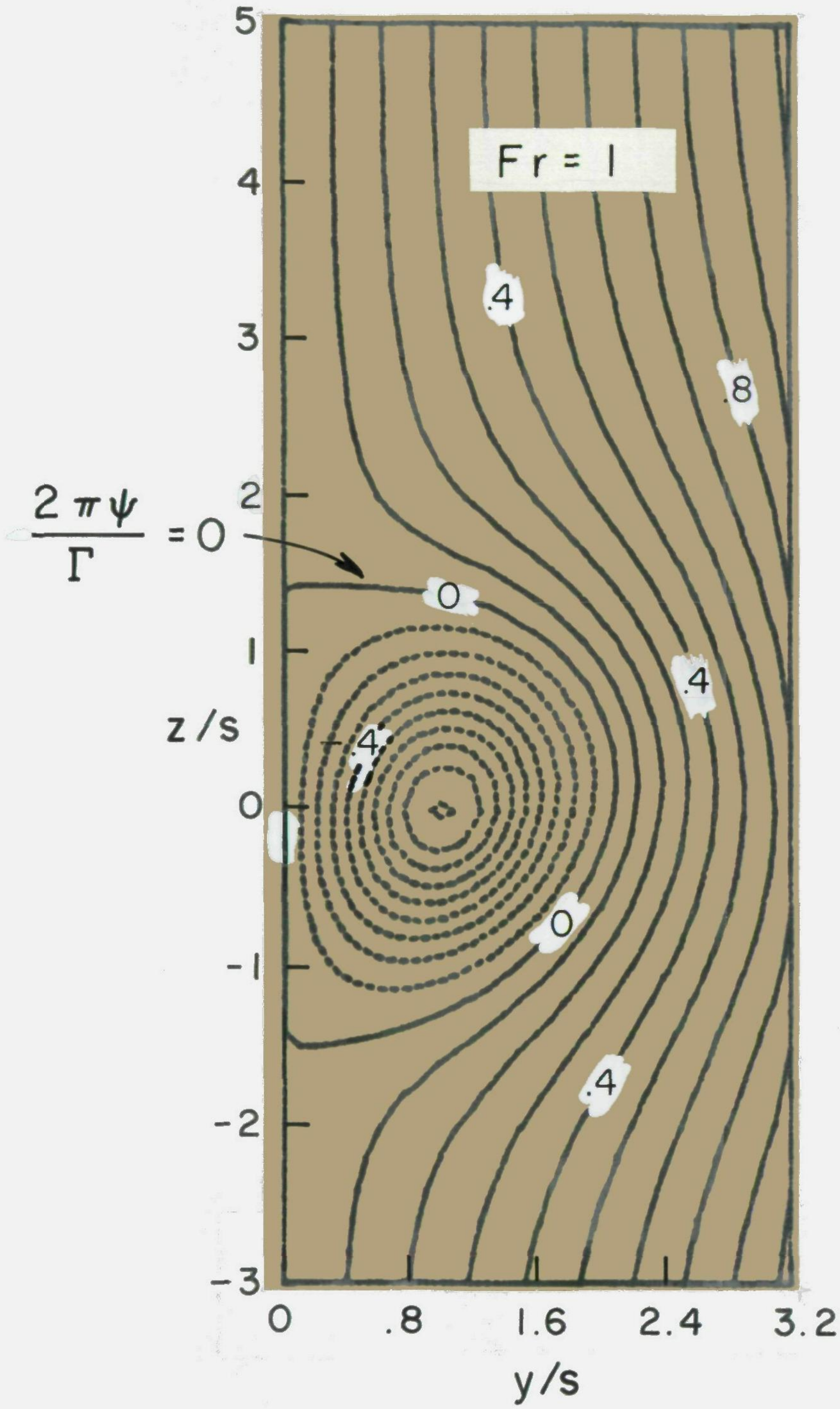

Figure 4.7 (b). Streamline pattern at $t\Gamma/2\pi s^2 = 1$
Contour interval = 0.1 , descent velocity
$-\frac{d\bar{z}}{dt}\frac{2\pi s}{\Gamma} = 0.35$.

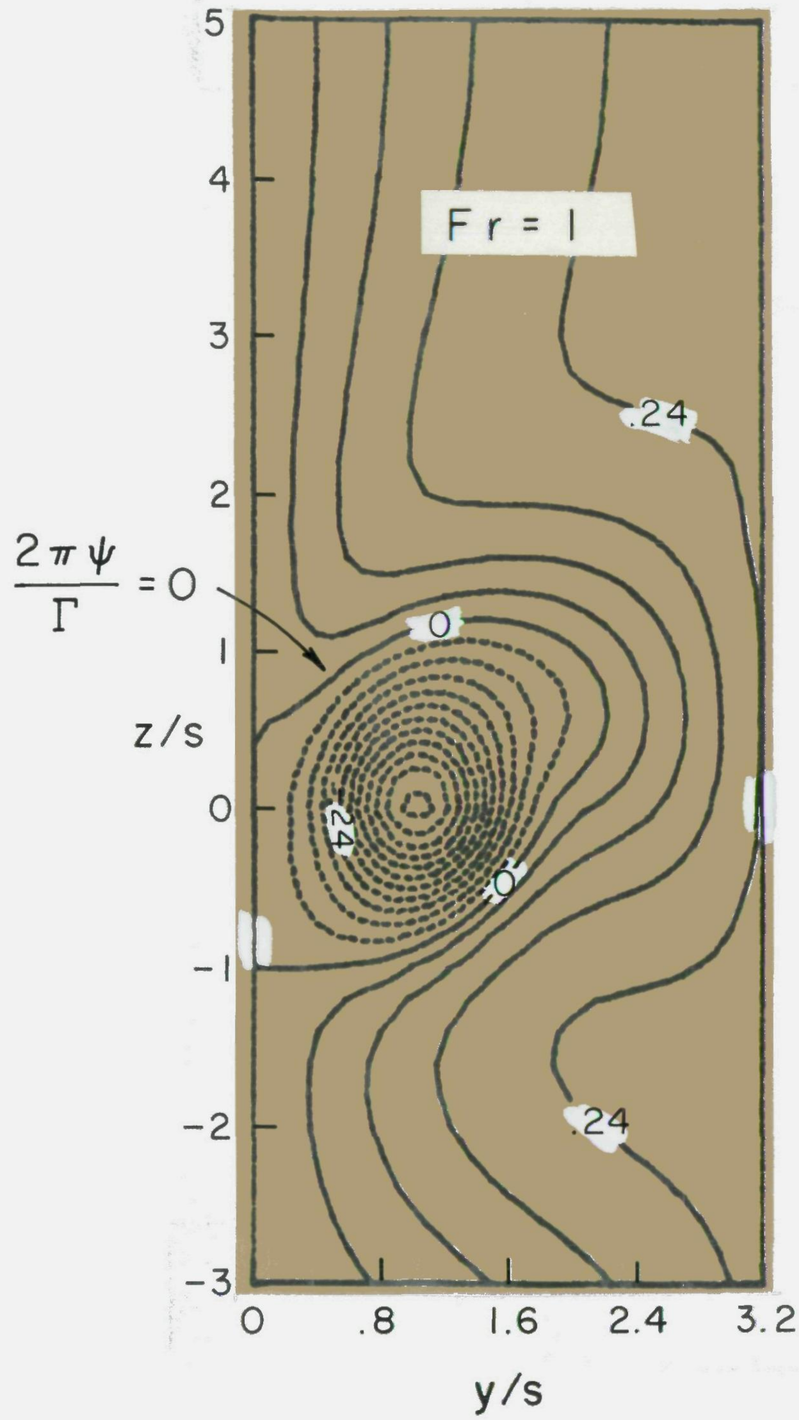

Figure 4.7 (c). Streamline pattern at $t\Gamma/2\pi s^2 = 1.68$, contour interval = 0.06, descent velocity $-\frac{d\bar{z}}{dt}\frac{2\pi s}{\Gamma} = 0.08$.

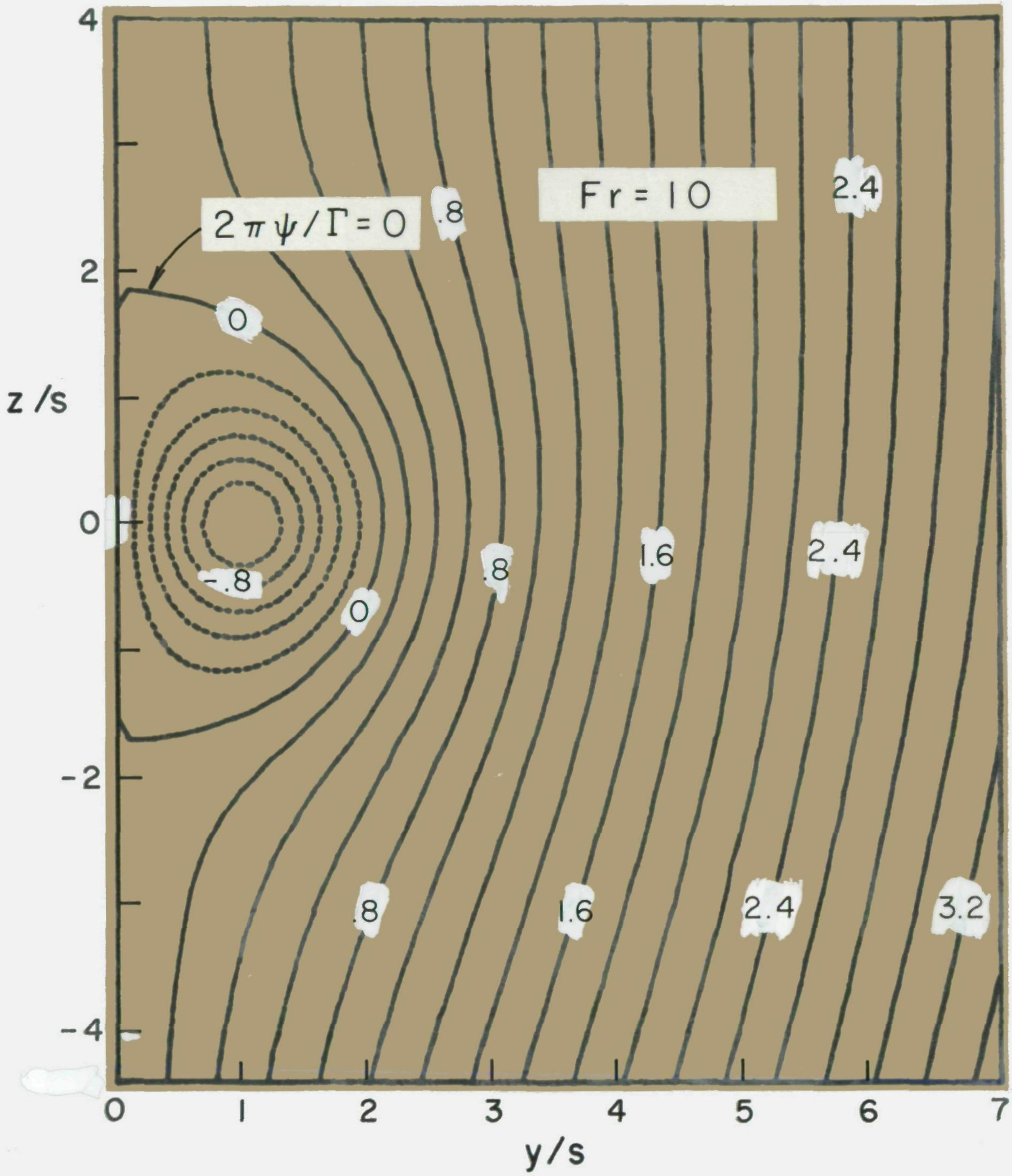

Figure 4.8 (a). Streamline pattern at $t\Gamma/2\pi s^2 = 0$, contour interval = 0.2 , descent velocity $-\frac{d\bar{z}}{dt}\frac{2\pi s}{\Gamma} = 0.5$.

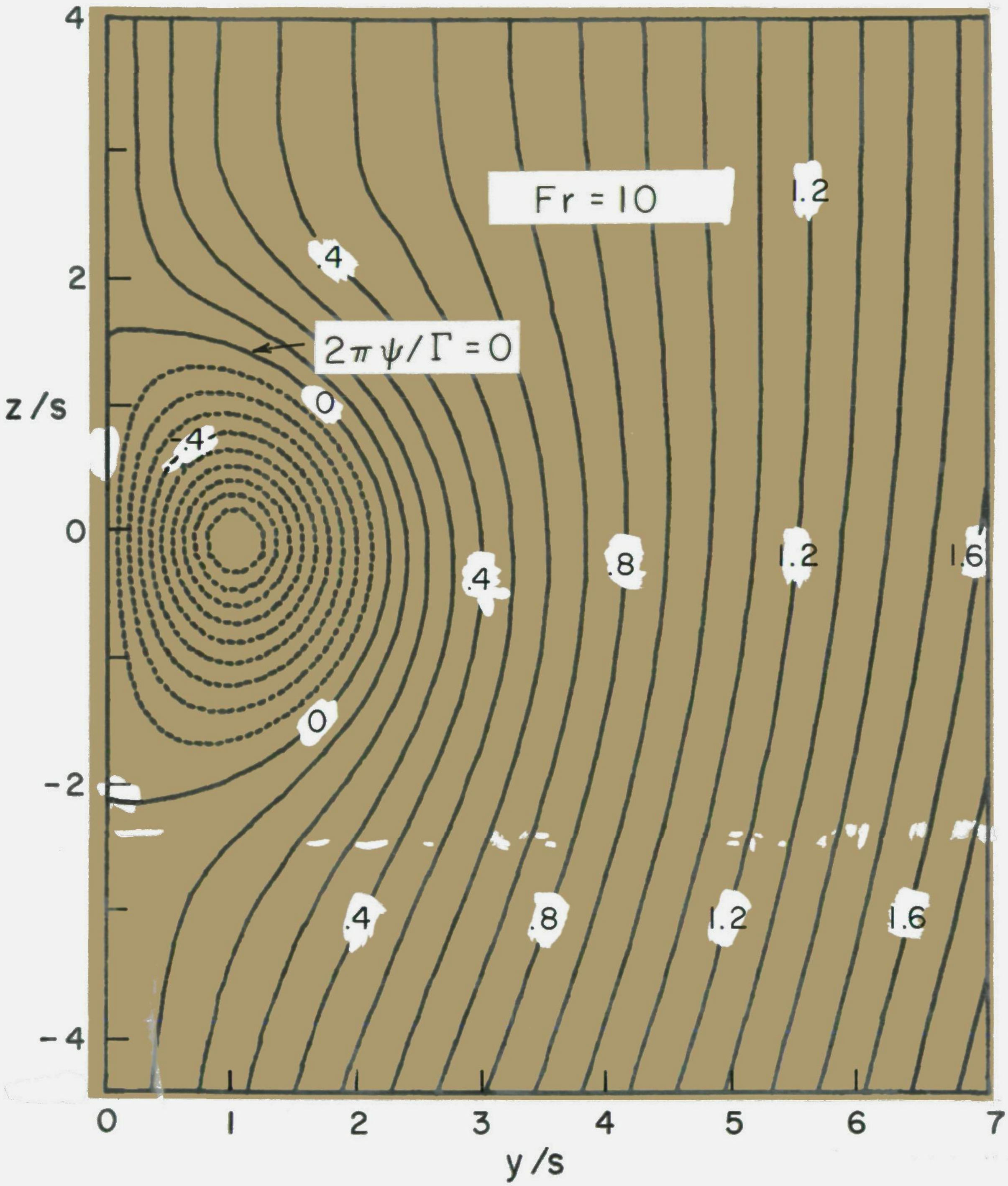

Figure 4.8 (b). Streamline pattern at $t\Gamma/2\pi s^2 = 16$, contour interval = 0.1, descent velocity $-\frac{d\bar{z}}{dt}\frac{2\pi s}{\Gamma} = 0.29$.

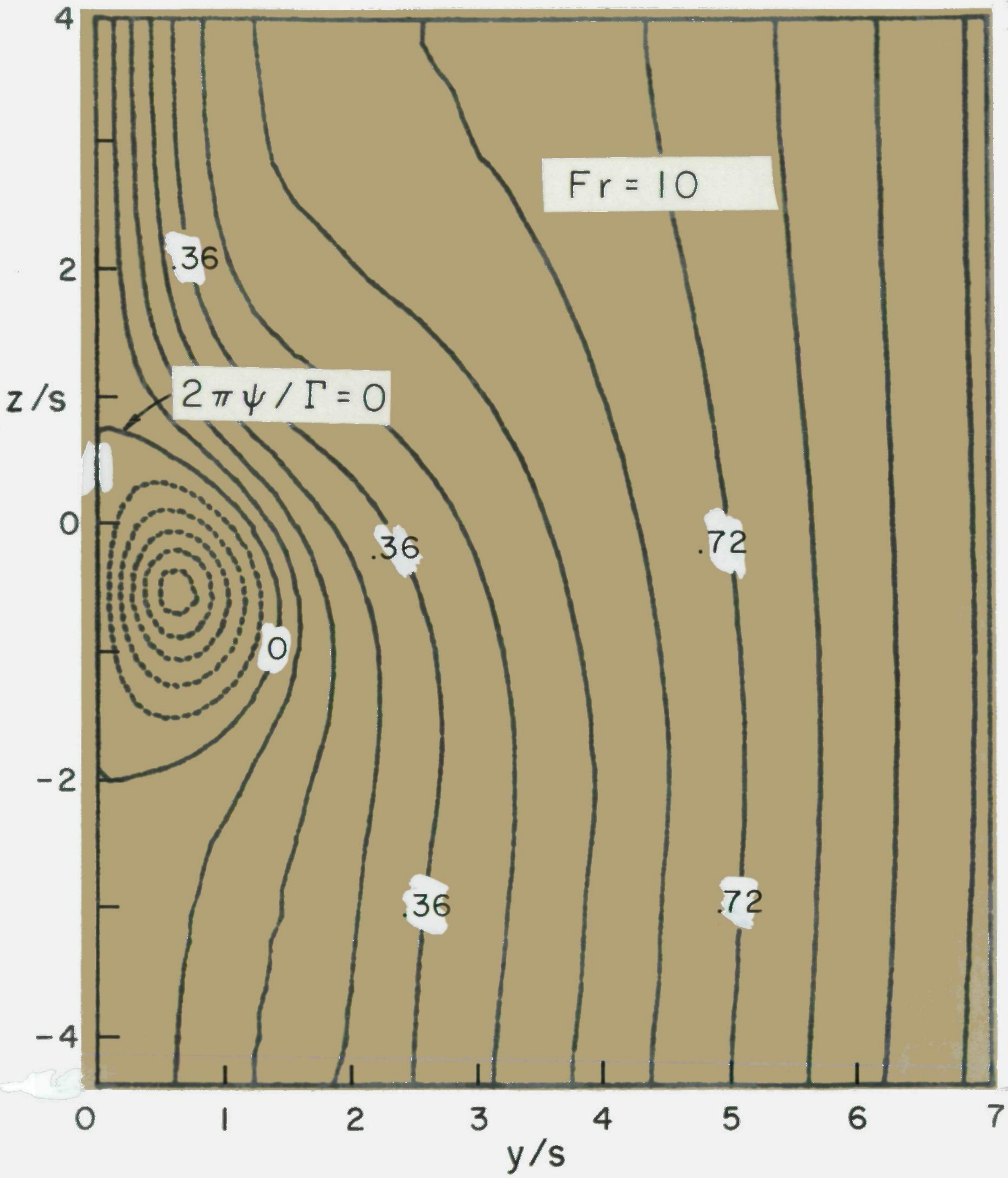

Figure 4.8 (c). Streamline pattern at $t\Gamma/2\pi s^2 = 28$, contour interval = 0.09, descent velocity $-\frac{d\bar{z}}{dt}\frac{2\pi s}{\Gamma} = 0.12$.

$$P.E._{max} = - \frac{g\Delta\rho}{2} \bar{z}_{max} \tag{4.7}$$

$\Delta\rho$ in a linear stratification at the point of maximum descent is

$$\Delta\rho = + \frac{d\rho_o}{dz} \bar{z}_{max} \tag{4.8}$$

With the assumption that the final oval area A is equal to the initial area, and that the oval area is given approximately by that of an ellipse having semi-axes of a translating point vortex pair

$$A = \pi(1.73)(2.09)s^2 \tag{4.9}$$

we find that the upper limit on the maximum descent of a vortex pair in a linear stratification, assuming constant oval area, is

$$\frac{\bar{z}_{max}}{s} = - 1.65\beta^{1/2} Fr \tag{4.10}$$

N is the Brunt-Väisälä circular frequency in rad/sec

$$N = - \left(\frac{g}{\rho_o} \frac{d\rho_o}{dz}\right)^{1/2} \tag{4.11}$$

Figure 4.9 shows a comparison between the maximum descent predicted by the theoretical upper limit and the results of a number of WAKE calculations. Both the approximate nature of this analysis and the fact that the numerical calculations contain self-induced turbulent dissipation, result in the discrepancy between numerical computation and the energy penetration argument. This discrepancy increases as Froude number increases since the self-induced turbulence becomes a progressively more important factor in decelerating the pair the longer the descent period. The presence of ambient turbulence in the atmosphere also places a limit on the maximum descent, independent of the stratification, see Donaldson and Bilanin Ref. 17. There, an approximate expression for the maximum descent of a vortex pair through a turbulent atmosphere is found to be

$$\frac{\bar{z}_{max}}{s} \simeq \frac{2.38}{(q/V_o)} \tag{4.12}$$

Thus, for an ambient turbulence level of $q^2/V_o^2 = 0.01$, the maximum

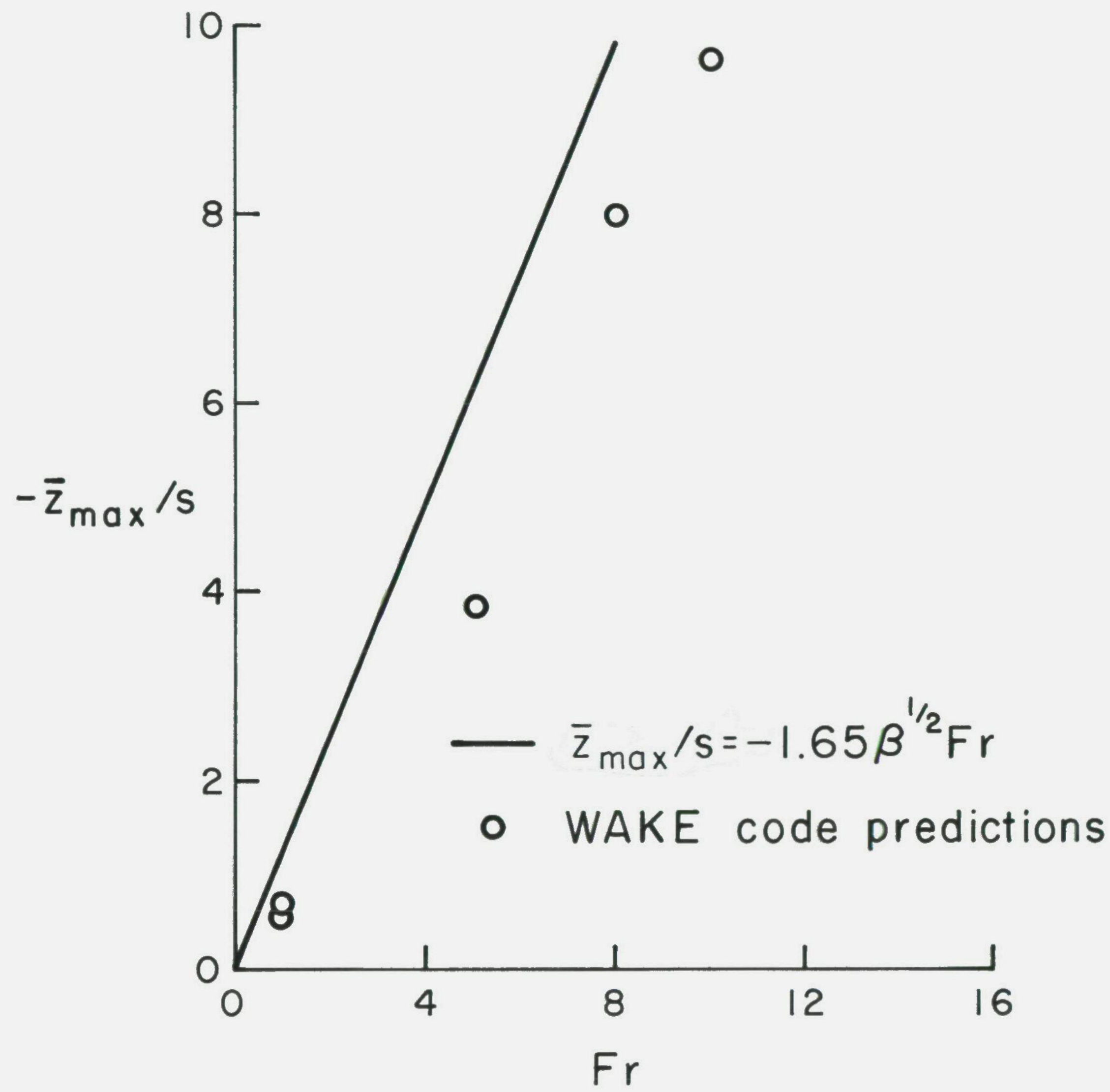

Figure 4.9. Maximum penetration of a vortex pair in a linearly stratified incompressible atmosphere.

descent in an unstratified environment is approximately $|\tilde{z}_{max}/s| = 24$ at $Fr = \infty$.

The penetration model posed here appears to yield a simple conservative means of estimating the maximum descent of a vortex pair in a linearly stratified atmosphere.

5. VORTEX INTERACTIONS IN A WIND TUNNEL AND WAKE ROLL UP

In this section two computations are described which demonstrate WAKE's ability to simulate flowfields in wind tunnels and to compute the roll up of a sheet of vorticity.

5.1 Simulation of the Cross Flow in a Rectangular Wind Tunnel.

It is anticipated that vortex wake flowfield data will be taken in wind tunnels with rectangular cross section. In addition, experiments have been carried out in NASA Langley's Long Track to investigate vortex ground plane interaction. To demonstrate that the WAKE code can be adapted to compute these flowfield configurations, a sample calculation was undertaken of the ascent of two equal strength vortices of opposite sign in a square enclosure.

The calculation simulates a square tunnel with walls located at $y/s = \pm 1.0$, $z/s = \pm 1.0$, and the flow is initialized with two Gaussian vortices of the form

$$\frac{2\pi s^2}{\Gamma} \eta = \pm 4.0 e^{-(r/s)^2/(0.16)^2} \qquad (5.1)$$

located at $z/s = 0$, $y/s = \pm 0.31$, respectively, in a uniform background turbulence of magnitude $(2\pi s/\Gamma)^2 q^2 = 0.01$. The turbulent scale is initialized as $\Lambda/s = 0.2$, the Reynolds number is 10^4 and the numerical grid is uniform in both directions with a spacing of $\Delta y/s = \Delta z/s = 1/16$. The law of the wall boundary condition, described in section 2, is applied at all four walls. Isopleths of the vorticity field at three times $t\Gamma/2\pi s^2 = 0$, 5.0 , 9.0 are shown in Figs. 5.1 - 5.3. Note that the vortex pair is self-induced to move upwards and produces vorticity of opposite sign on the wind tunnel walls. Note also that this simulation could have been run using half the mesh points if the symmetry of the solution had been utilized.

5.2 Roll Up of a Vortex Sheet

The vorticity that is shed from the trailing edge of a wing is initially a vortex sheet which then rolls up into discrete vortices. The difficulties of computing sheet roll up by finite difference are tied to the problem of the high numerical resolution required to resolve the sheet of vorticity. To check to see if finite difference is a feasible technique, a sample calculation has been performed. Assume there exists a parabolical load distribution on a wing such that

$$\Gamma/\Gamma_o = 1 - (y/s)^2 \quad , \quad |y| < s \qquad (5.2)$$

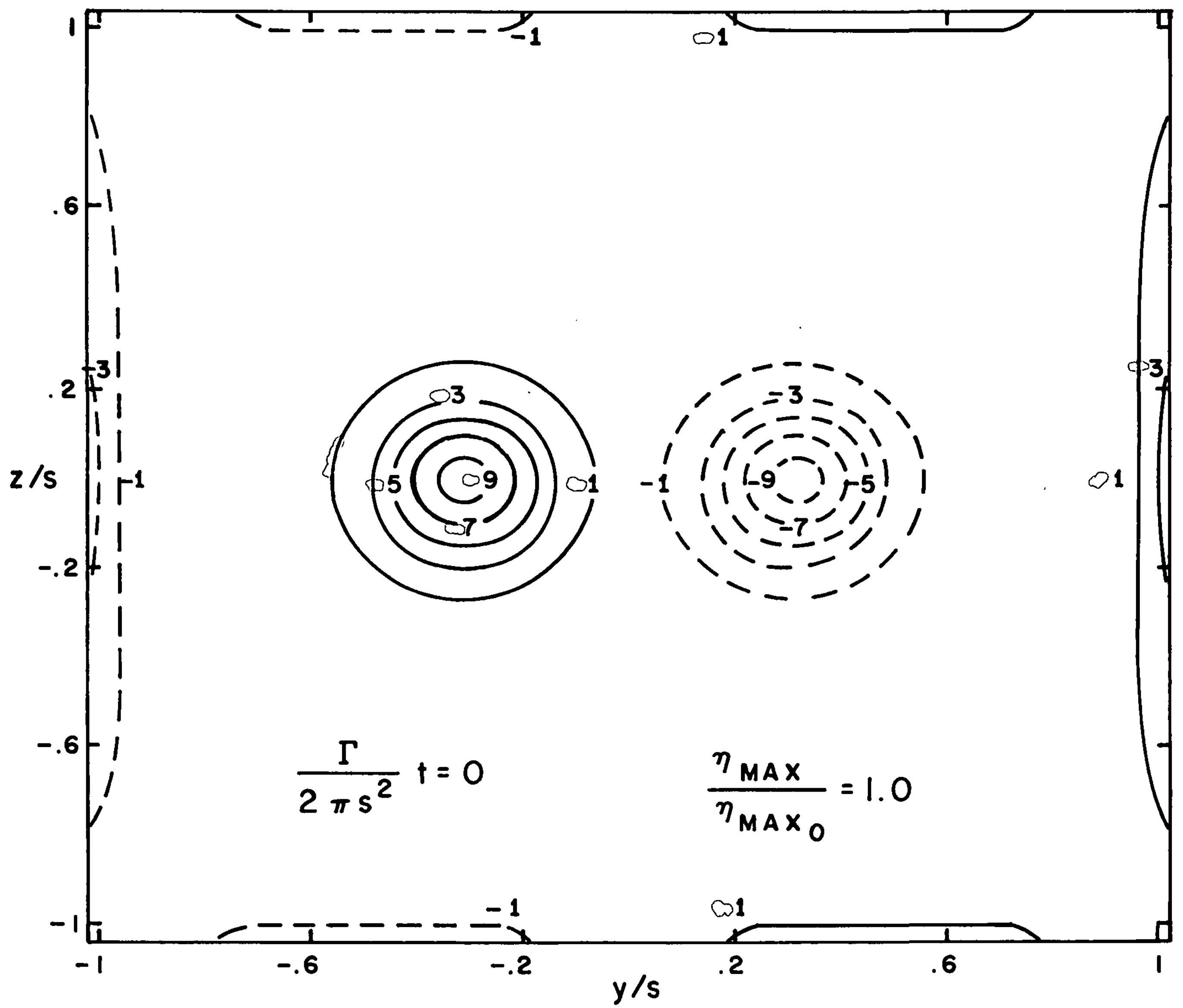

Figure 5.1. Isopleths of vorticity, labels on the curves are ten times the fraction of the maximum value.

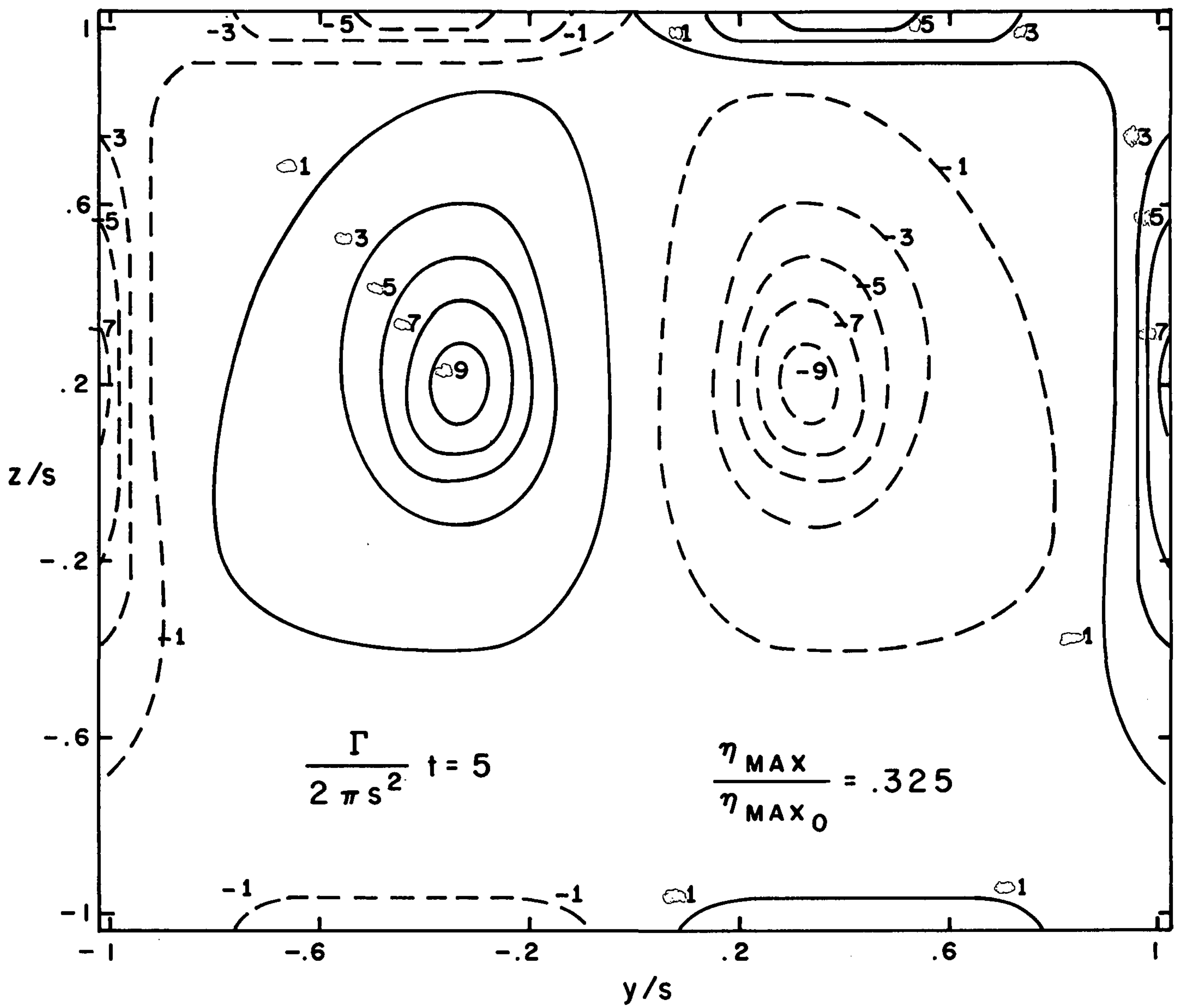

Figure 5.2. Isopleths of vorticity, labels on the curves are ten times the fraction of the maximum value.

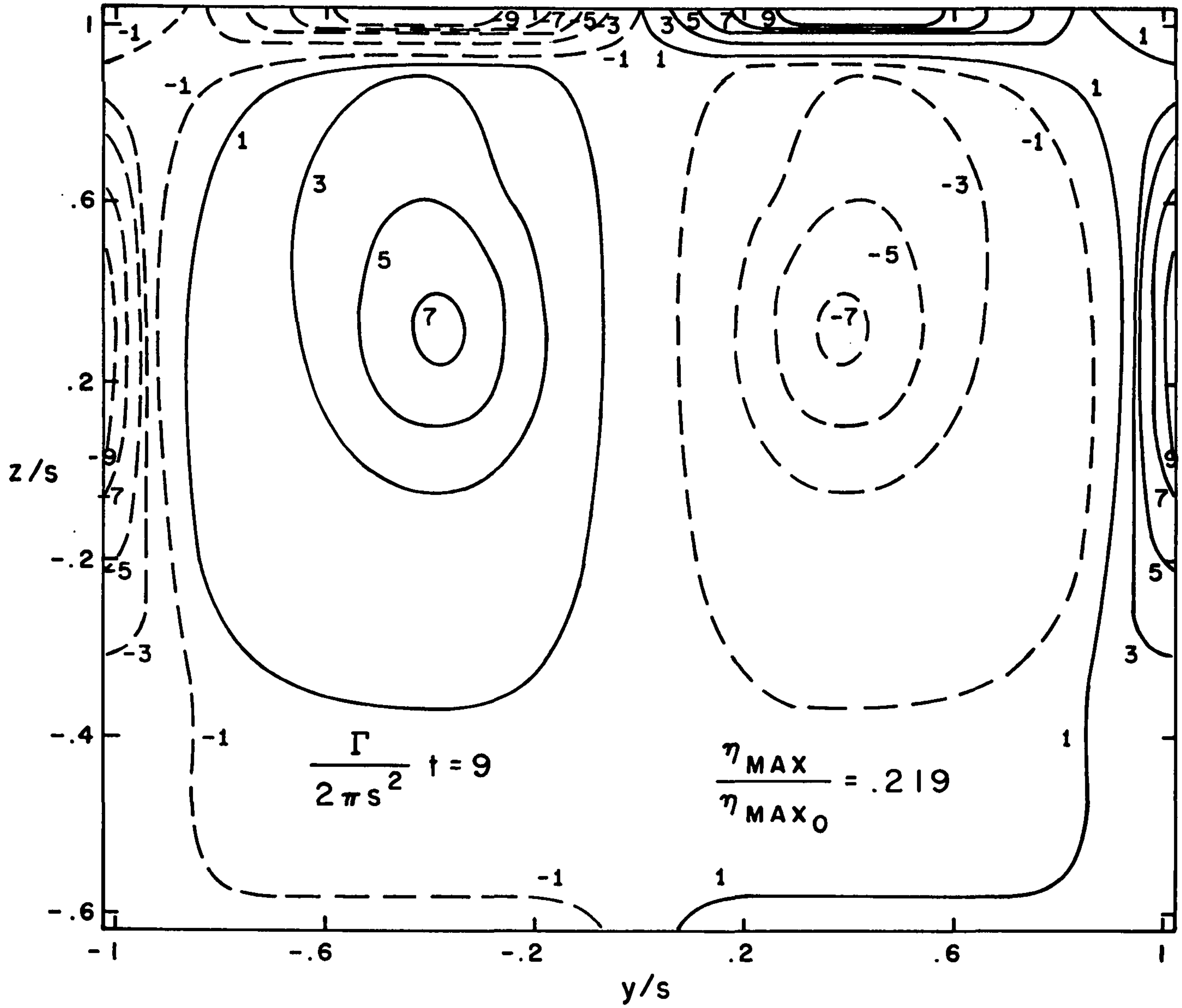

Figure 5.3. Isopleths of vorticity, labels on the curves are ten times the fraction of the maximum value.

Then the sheet strength is

$$\gamma = -\, d\Gamma/dy = \begin{cases} -\,2y\Gamma_o/s^2 & , \quad |y| < s \\ 0 & , \quad \text{otherwise} \end{cases} \tag{5.3}$$

If it is assumed that the vorticity distribution is a Gaussian of width σ in the z direction, then

$$\eta s^2/\Gamma_o = \begin{cases} \dfrac{2y}{\sqrt{\pi}\,\sigma}\, e^{-(z/\sigma)^2} & , \quad |y| < s \\ 0 & , \quad \text{otherwise} \end{cases} \tag{5.4}$$

This vorticity distribution with $\sigma/s = 0.05$ was used to initialize a laminar WAKE simulation with a Reynolds number of $Re = 200$. The numerical domain was specified to be $0 < y/s < 2.0$, $-2.0 < z/s < 2.0$, with a resolution of $\Delta y/s = 0.0625$ and $\Delta z/s = 0.105$. The time evolution of the vortex roll up is shown in Figs. 5.4 - 5.9 as isopleths of the vorticity in the cross flow plane. At a non-dimensional time of approximately 5, roll up is complete and an "axisymmetric" structure has evolved. Note the difference between the y/s and z/s scales.

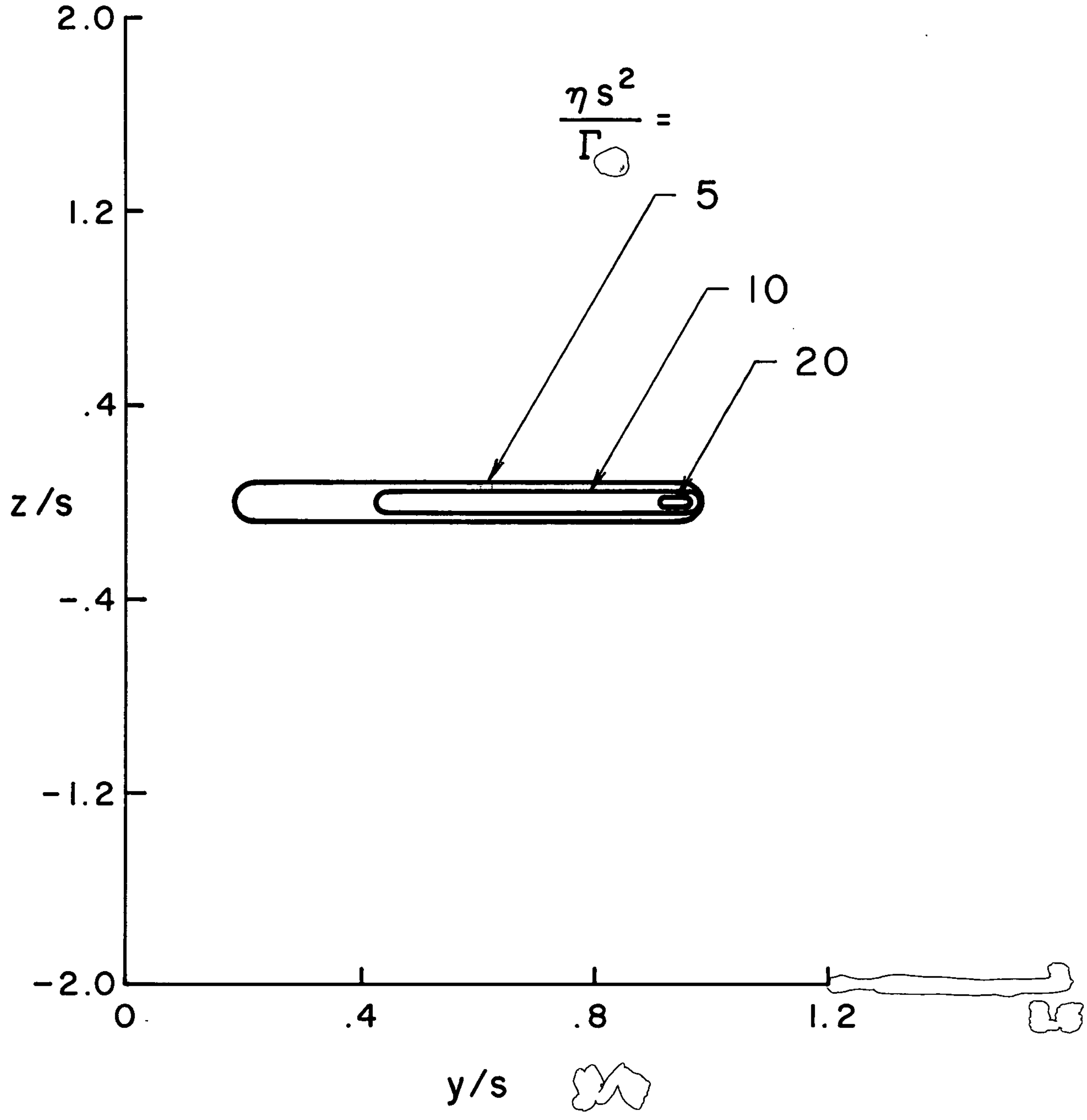

Figure 5.4. Vortex Sheet Roll Up - Isopleths of Vorticity

$$\frac{\Gamma}{2\pi s^2} t = 0$$

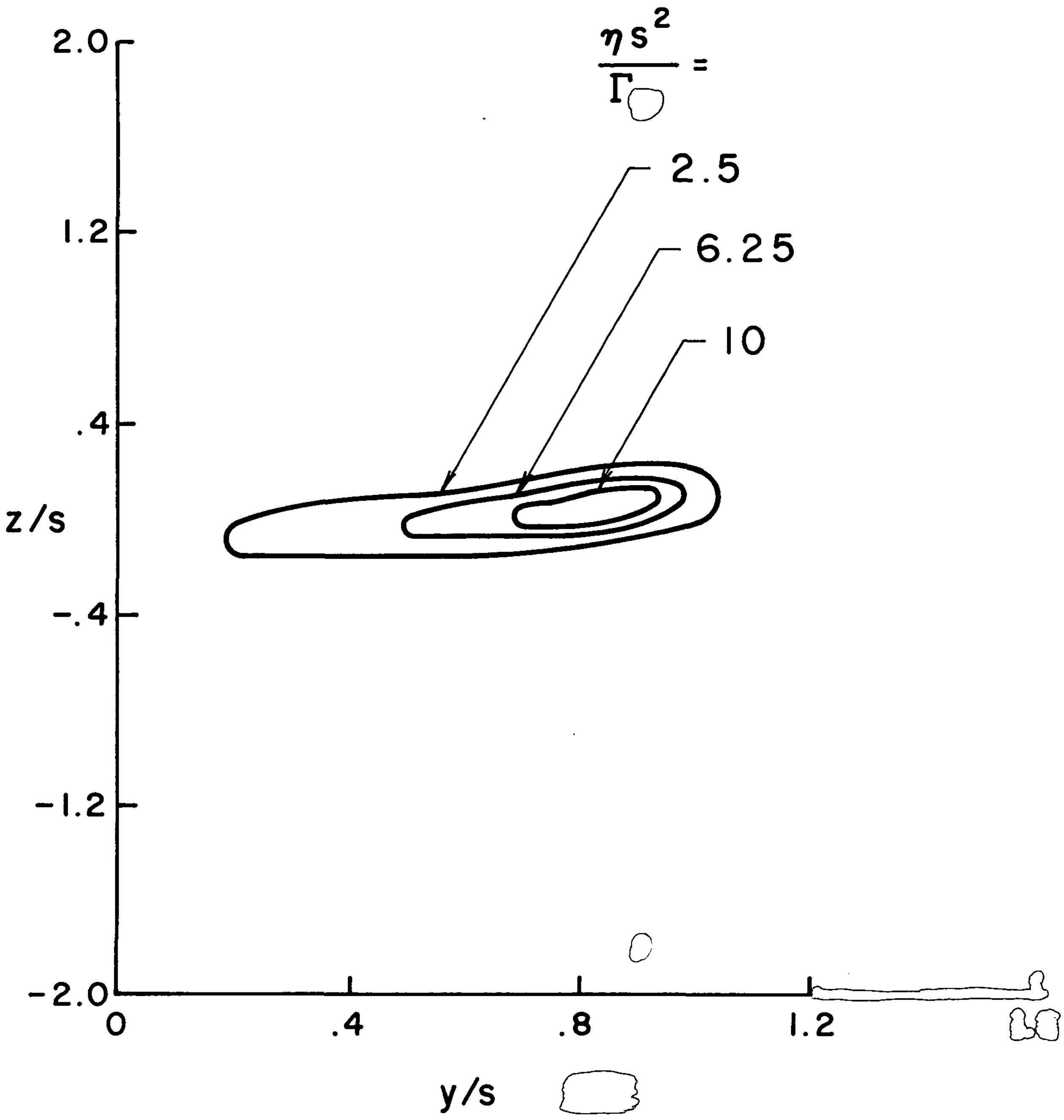

Figure 5.5. Vortex Sheet Roll Up - Isopleths of Vorticity

$$\frac{\Gamma}{2\pi s^2} t = 0.186 .$$

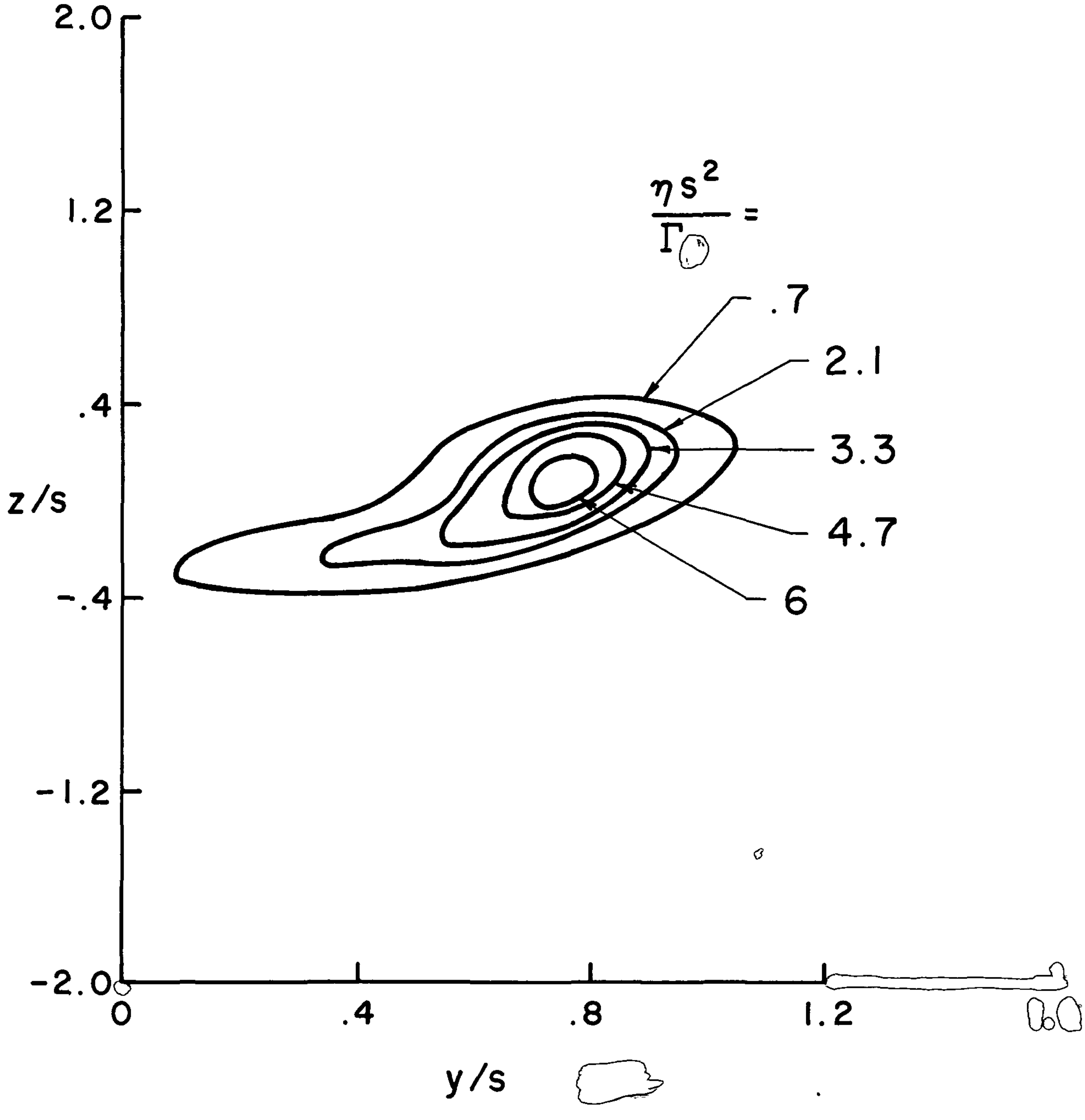

Figure 5.6. Vortex Sheet Roll Up - Isopleths of Vorticity

$$\frac{\Gamma}{2\pi s^2} t = 0.859 .$$

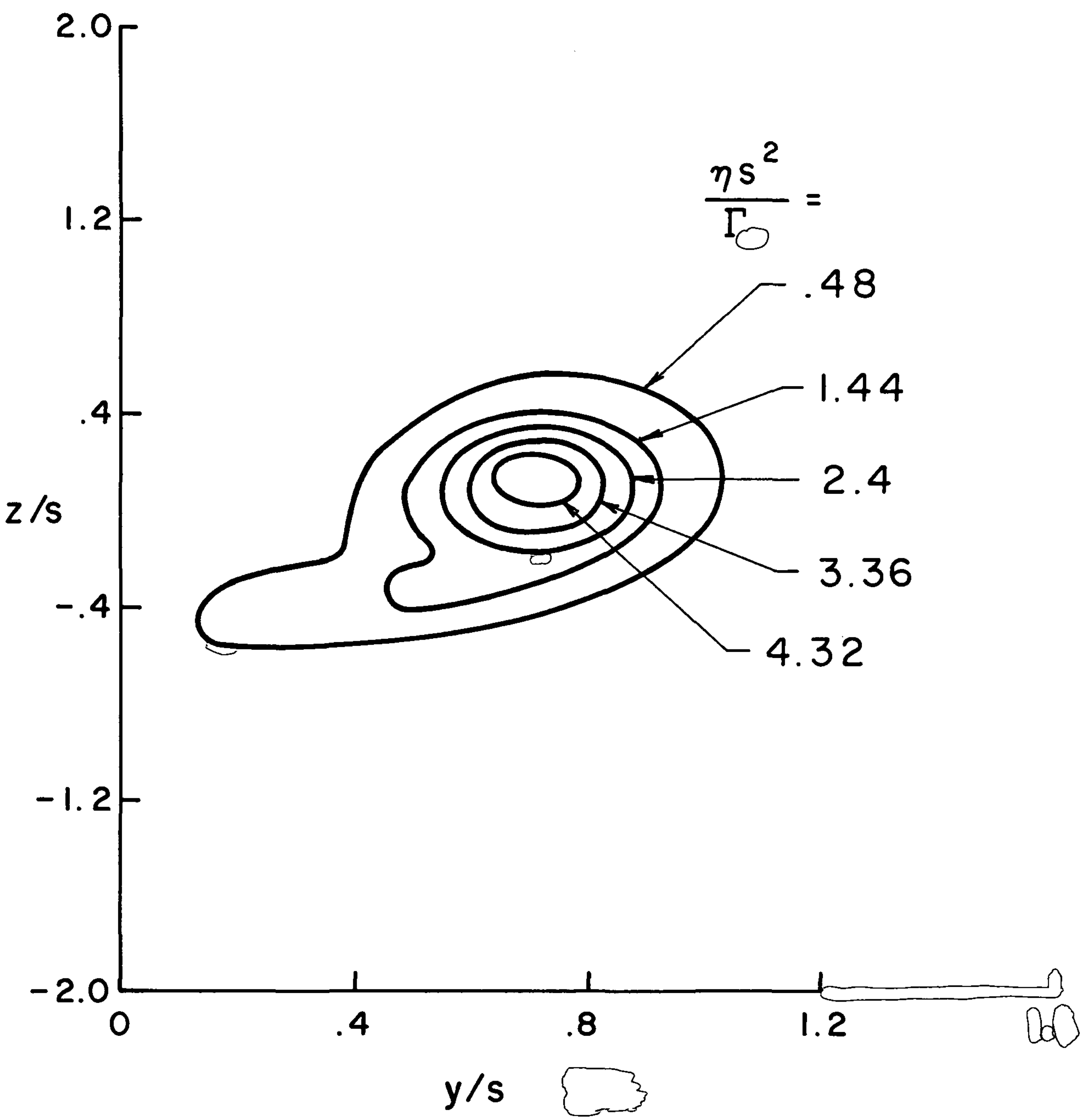

Figure 5.7. Vortex Sheet Roll Up - Isopleths of Vorticity

$\frac{\Gamma}{2\pi s^2} t = 1.53$.

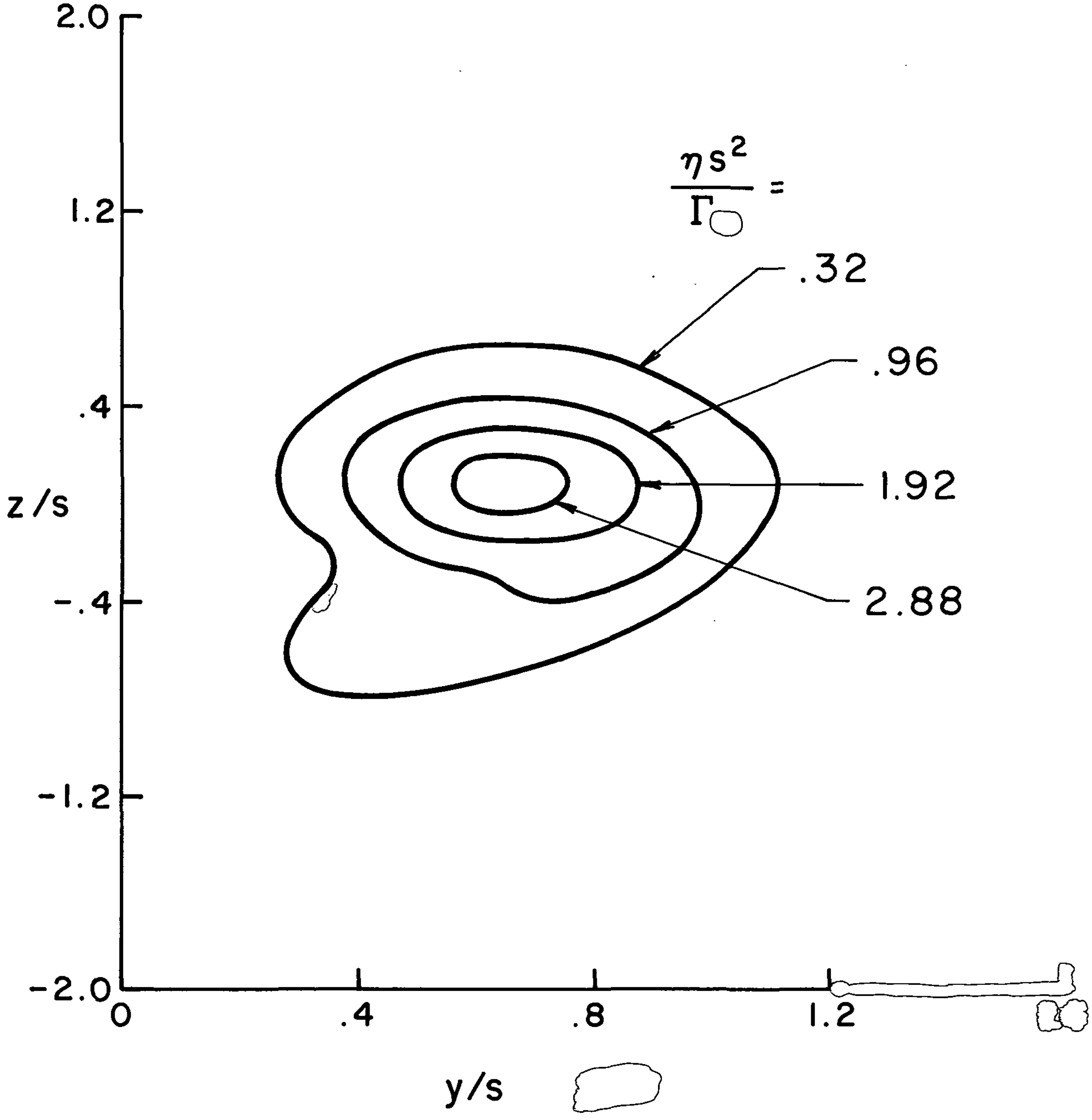

Figure 5.8. Vortex Sheet Roll Up - Isopleths of Vorticity

$$\frac{\Gamma}{2\pi s^2} t = 2.92 .$$

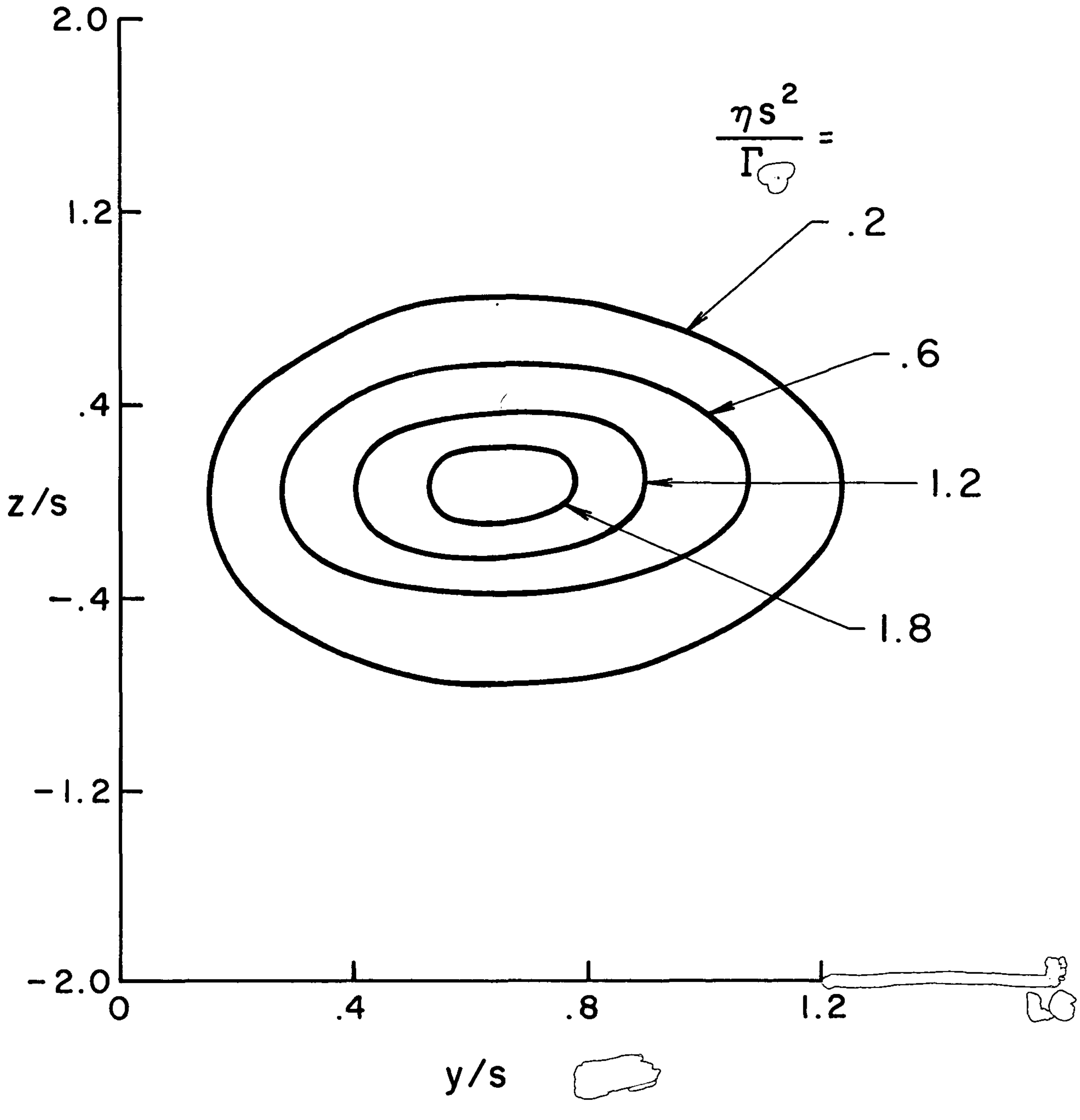

Figure 5.9. Vortex Sheet Roll Up - Isopleths of Vorticity

$$\frac{\Gamma}{2\pi s^2} t = 5.43 .$$

6. CONCLUSIONS AND RECOMMENDATIONS

Several conclusions from this study can be made with regard to the ability of the atmosphere to dissipate aircraft vortex wakes.

1. After vortex interactions in multiple vortex pair wakes have gone to completion, the resulting vortex pair in the absence of atmospheric effects is predicted to decay very slowly. Direct computation has shown that the circulation in a fixed contour and the rolling moment induced on an encountering aircraft decay asymptotically for large times as $t^{-1/2}$.

2. The presence of ambient background turbulence in a neutral atmosphere has a strong influence on the decay rate of a vortex pair. Direct computation has shown that asymptotically for large time, the circulation in a fixed contour and the rolling moment induced on an encountering aircraft decay as t^{-2}. More detailed predictions of the decay rate must include specification of the integral scale of turbulence if comparisons are to be made with measured data.

3. Crosswind shear results in the observed solitary vortex phenomenon. The vortex whose vorticity is of the sign opposite to that vorticity in the shear is dispersed. The decay of the solitary vortex is dependent on the amount of ambient turbulence associated with the shear. It is postulated that under stable conditions, where shear can be present without turbulence, the solitary vortex may persist for a long time.

4. The classic picture of a vortex pair descending towards a ground plane following a hyperbolic trajectory is shown to be incorrect. Viscous interaction with the ground plane results in the generation and separation of secondary vorticity from the ground. This secondary vorticity reduces the strength of the vortex wake as well as results in a rebounding or bouncing of the pair away from the ground.

5. A vortex pair descending into a stably stratified incompressible atmosphere is shown to have a finite penetration dependent upon the severity of the stratification. It is suggested that proper accounting of turbulent transport is as important as proper accounting for the buoyancy produced vorticity in predicting the dissipation of a vortex pair in a stably stratified fluid. A major finding is that once a vortex pair's descent is halted by stratification, the vortex is still capable of inducing a significant rolling moment on an encountering aircraft of a span less than or equal to the generator's span.

6. Lastly, sample calculations have shown that the WAKE code can be used to compute the initial sheet roll up as well as to simulate vortex flows in rectangular enclosures. This capability should prove useful in future wake related work.

The results obtained from this study warrant the following recommendations.

It is becoming increasingly apparent that the WAKE code has the potential of being an invaluable predictive tool in flow situations where it is impractical or even impossible to make measurements. The code's usefulness is, however, limited until proper validation against vortex related data can be completed. It is strongly recommended that a set of experiments be devised which will produce sufficient data appropriate to validate the WAKE code.

Results of analytic studies reported here suggest that the atmosphere plays a powerful role in affecting the dissipation of aircraft vortex wakes. No comparison is directly made with data. The Department of Transportation, as part of their effort in the vortex hazard program, has monitored the descent of thousands of vortex wakes under various atmospheric conditions. It is suggested that a review of these data and correlation against predictions made herein will increase our understanding of the ability of the atmosphere to dissipate vortex wakes.

APPENDIX

Presented at the 16th Aerospace Sciences Meeting, Huntsville, Alabama, January 17, 1978.

THE ROLE OF ATMOSPHERIC SHEAR, TURBULENCE AND A GROUND PLANE ON THE DISSIPATION OF AIRCRAFT VORTEX WAKES

A. J. Bilanin,* M. E. Teske† and J. E. Hirsh°
Aeronautical Research Associates of Princeton, Inc.
50 Washington Road, Princeton, New Jersey 08540

Abstract

Enhanced dispersion of two-dimensional trailed vortex pairs within simplified neutral atmospheric backgrounds is studied numerically for three conditions: when the pair is imbedded in a constant turbulent bath (constant dissipation); when the pair is subjected to a mean cross-wind shear; and when the pair is near the ground. Turbulent transport is modeled using second-order closure turbulent transport theory. The turbulent background fields are constructed using a superequilibrium approximation. The computed results allow several general conclusions to be drawn with regard to the reduction in circulation of the vortex pair and the rolling moment induced on a following aircraft: (1) the rate of decay of a vortex pair increases with increasing background dissipation rate; (2) cross-wind shear disperses the vortex whose vorticity is opposite to the background; and (3) the proximity of a ground plane reduces the hazard of the pair by scrubbing. The phenomenon of vortex bounce is explained in terms of secondary vorticity produced at the ground plane. Qualitative comparisons are made with available experimental data, and inferences of these results upon the persistence of aircraft trailing vortices are discussed.

Nomenclature

C	passive tracer $(C^* = C/C_o)$
C_ℓ	proportional to the induced rolling moment, Eq. (3)
q	root mean square of the turbulent kinetic energy $(q^* = q2\pi s/\Gamma_o)$
r	radial coordinate measured from vortex center
s	initial semiseparation between vortices
t	time $(t^* = t\Gamma_o/2\pi s^2)$
U_i	mean Cartesian velocity components
$\langle u_i u_j \rangle$	ensemble averaged Reynolds stress correlation
x_j	Cartesian coordinates
z_o	hydrodynamic roughness length
β	normalized constant cross shear $(2\pi s^2/\Gamma_o)\partial V/\partial z$
Γ_o	initial circulation
ε	turbulent dissipation rate $(\varepsilon^* = (2\pi)^3 s^4 \varepsilon/\Gamma_o^3)$
ζ	streamwise component of vorticity $(\zeta^* = \zeta 2\pi s^2/\Gamma_o)$
Λ	turbulent macroscale parameter
ν	kinematic viscosity
σ	vortex spread parameter
ψ	streamfunction

* Senior consultant, Member AIAA
† Consultant
° Associate Consultant

Introduction

The decay of aircraft vortex wakes has been the focus of extensive investigation by both NASA and DOT, in an effort to determine hazard potential and wake lifetime. Because of the inherent difficulty in making measurements in the wakes of aircraft, investigations have included the development of computer codes to simulate vortex behavior and predict vortex interaction. The work described herein are results from one such code "VORTEX WAKE."

Donaldson and Bilanin[1] present a review of the physics underlying vortex generation and decay, and the approaches used to analyze these effects. A comprehensive review of the entire subject has recently been given by Hallock and Eberle.[2] In Bilanin, Teske and Williamson[3] (hereafter referred to as "I"), we used the point-vortex approach of Rossow[4] to initiate a discussion of vortex merging, wherein vortices of like sign interact. The thrust in I was the application of turbulent transport theory to the merging process, to provide for a complete description of the convective and dissipative processes within the vortices themselves. The two-dimensional, unsteady numerical code, "VORTEX WAKE," programs the Reynolds stress equations modeled by Donaldson.[5] The formulation of the modeled equation and the numerical procedures involved in solving them are included in I, as is an extensive discussion of the merging of multiple trailing vortices and the minimum hazard potential for a wing.

One important result from I is that a pair of oppositely-signed vortices exhibit a surprisingly slow rate of decay when descending in a calm, neutral atmosphere

Copyright © American Institute of Aeronautics and Astronautics, Inc., 1978. All rights reserved.

away from the ground. These ideal conditions, fortunately, are not met often in practice. More commonly, vortex pairs encounter background turbulence, mean wind gradients, or the ground while descending in an atmosphere which is not in general neutrally stable. The effects of background turbulence, wind shear and ground interaction form the subject of this paper. Here, we will demonstrate through the use of our turbulent transport code that any of these quite naturally occurring effects may substantially reduce the lifetime of a vortex pair. Descent of a vortex pair in a stably stratified atmosphere will be the subject of a subsequent paper.

In Section II, we briefly review the turbulent transport model and examine the superequilibrium limit of this model which is used to provide idealized atmospheric environments. Also, improvements in the numerical code are discussed here.

In Section III, we examine the effects of background turbulence on a vortex pair, showing that decay increases with increasing dissipation rate. In Section IV, we investigate the effects of mean shear and offer an explanation of the "solitary" vortex phenomenon. Finally, in Section V, we investigate vortex interaction with a ground plane and explain the phenomenon of vortex bounce which has been observed on runways and in subscale tests.

II. The Turbulence Model and "Vortex Wake" Code

A need to predict turbulent transport in rapidly rotating, as well as stratified flows, led Donaldson to develop a second-order closure model of turbulent transport. A second-order model implies that partial differential equations are solved for the Reynolds stress tensor $\langle u_i u_j \rangle$ as well as for the mean ensemble averaged U_i velocity components. Higher-order unknowns and certain second-order correlations in the Reynolds stress equations are replaced by modeled terms containing constants and second-order correlations. These constants are evaluated by comparison with measurements made of fundamental fluid flows. A complete summarization of the current state of incompressible modeling as used here may be found in Lewellen and Teske.[6] The computations which follow idealize the neutral atmosphere by assuming constant shear and homogeneous turbulence in the absence of a vortex wake. The background turbulence levels are determined by the "superequilibrium" limit of the turbulent transport model.[5] Superequilibrium limit is that turbulent fluid state which is approached at high Reynolds number when time rates of change and diffusion of second-order correlations are negligible. When the diffusion and rate terms are set equal to zero in the rate equations for the second-order velocity correlations and a high Reynolds number is assumed, the resulting Reynolds stress equations for $\langle u_i u_j \rangle$ may be written as:

$$0 = \overbrace{-\langle u_i u_k \rangle \frac{\partial U_j}{\partial x_k} - \langle u_k u_j \rangle \frac{\partial U_i}{\partial x_k}}^{\text{production}} \underbrace{- \frac{q}{\Lambda}\left(\langle u_i u_j \rangle - \delta_{ij}\frac{q^2}{3}\right)}_{\text{tendency towards isotropy}} \underbrace{- \frac{q^3}{12\Lambda}\delta_{ij}}_{\text{isotropic dissipation}} \quad (1)$$

where $q^2 = \langle u_i u_i \rangle$ and Λ is the turbulent macroscale. The production terms in (1) are balanced by a Rotta tendency-towards-isotropy term and an isotropic dissipation term. If the principle gradient is in the z-direction for the U velocity, for instance, then it may be shown that the solution to (1) is

$$\begin{aligned} q^2 &= 2\left(\Lambda \frac{\partial U}{\partial z}\right)^2 \\ \langle uu \rangle &= \left(\Lambda \frac{\partial U}{\partial z}\right)^2 \\ \langle vv \rangle &= \langle ww \rangle = 0.5\left(\Lambda \frac{\partial U}{\partial z}\right)^2 \\ \langle uw \rangle &= -0.354\left(\Lambda \frac{\partial U}{\partial z}\right)^2 \\ \langle uv \rangle &= \langle vw \rangle = 0 \end{aligned} \quad (2)$$

In the vicinity of a ground plane, the velocity gradient is inversely proportional to z, (with z measured upwards from the ground) while the macroscale is proportional to z, maintaining a constant product of $\Lambda \partial U/\partial z$.

The mean and rate equations for the second-order equations correlations have been programmed into a two-dimensional unsteady incompressible computer code. The assumption of two-dimensionality implies that the phenomena to be investigated are such that axial gradients are insignificant and can be neglected. Therefore, sinusoidal instability and vortex breakdown are phenomena which cannot be addressed with this code.

The numerical solution technique (using an ADI scheme) is given in I. Several extensions to the code since the publication of I are the following. The mean equations have been reworked into streamfunction-vorticity variables, eliminating the need to compute the pressure. A direct solver developed by Swartztrauber and Sweet[7] determines the streamfunction, from which the velocity fields are obtained. In this way continuity is assured, even though a more difficult set of boundary conditions may sometimes result. To improve our simulation of the convective nature of the vortex flow problem, we now use a J_6 representation of the convective operator (Arakawa[8]), wherein the conservative and nonconservative operators are averaged.

For the specific computation of vortex pairs, an upwash velocity is added to keep the vortex pair in the computational domain. This is equivalent to sitting on the vortex pair as it descends. When the results are presented, however, the vertical coordinate is shifted to show the actual amount of descent which has resulted. The choice as to what defines the position of a vortex is arbitrary. In I the centroid of the vorticity distribution was used to define vortex location. This definition was adequate for vortex pair computations in the absence of a ground plane. As will be shown later, however, when vortices interact with a ground plane, vorticity of the opposite sign is generated at the ground. This additional vorticity limits the usefulness of the centroid concept to fix position. To overcome this difficulty a passive tracer (neutral smoke) is initially prescribed in the center of the vortex and the maximum of this passive tracer is taken as the vortex center. As the pairs spread by turbulent diffusion, readjustment of the numerical grid is undertaken to keep the boundaries away from the centers of vorticity. This readjustment does not cause any numerical problems.

As a convenience, initial distributions of vorticity, second-order turbulence quantities and passive tracer are taken to be Gaussian. To reduce grid point requirements, whenever possible, half-plane computations are made. A uniform mesh is used except near the ground where additional resolution is, in general, needed to define the large shears that exist there.

III. Vortex Pairs in Constant Turbulent Backgrounds

In I the decay of a vortex pair in a constant dissipation rate turbulent bath was investigated to show that the dissipation rate itself is not sufficient to determine the rate of decay of vortices. It was shown that in a neutrally stable atmosphere, in the absence of mean cross wind shear, both the integral scale of the turbulent eddies, Λ , and the turbulent dissipation rate, ε , must be specified to fix vortex wake decay rate. In this section, additional computations are described and simple decay laws are deduced from the computations.

The computations are initialized by positioning a Gaussian of vorticity of the form $\zeta 2\pi s^2/\Gamma_0 = \pm (2/\sigma^2) \exp(-(r/s)^2/\sigma^2)$ at $y/s = \pm 1$, $z = 0$, respectively. The coordinate, r , is measured radially outward from the vortex center and σ is the vortex spread, ($\sigma = 0.5$ for all computations). The numerical mesh is specified only for $y > 0$ since symmetries about $y = 0$ can be utilized. In addition to a uniform background level of turbulence an isotropic Gaussian spot of turbulence is positioned in the center of each vortex of strength $(q_0 2\pi s/\Gamma_0)^2 = 0.01$, such that $\langle uu \rangle = \langle vv \rangle = \langle ww \rangle = (q_0^2/3) \exp[-(r/s)^2/\sigma^2]$. When a passive tracer is used, it begins with the same Gaussian character and has strength $C_0 = 1$. At the edges of the computation domain, except at the $y = 0$ boundary, turbulent quantities are assumed to reach the superequilibrium state and tracer concentration is set equal to zero. The streamfunction is obtained from moment expansion of the Biot Savart law as described in I. The initial conditions are schematically shown in Fig. 1.

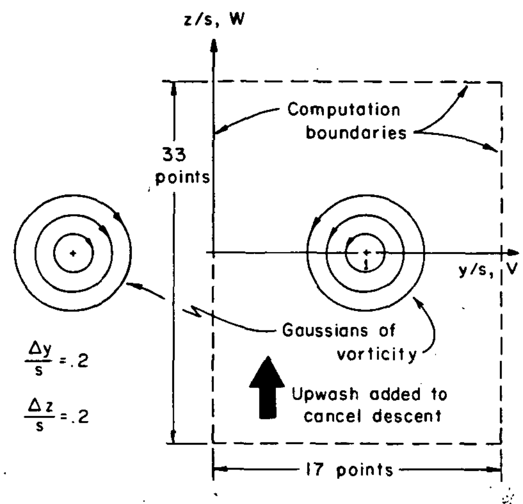

Figure 1. The initial conditions for the computation of the decay of a vortex pair in a neutrally stable turbulent atmosphere.

As a baseline computation the ambient turbulent field was set equal to zero and the decay of a vortex pair in a calm atmosphere was simulated. In this computation, as in all computations presented here unless otherwise noted, the integral scale parameter was initialized to be $\Lambda/s = 0.2$ and the Reynolds number was fixed at $\Gamma_0/\nu = 10^4$. The evolution of the scale is controlled by a dynamic scale equation detailed in I. As can be seen by examining the contour plots of vorticity for several times as shown in Fig. 2, a vortex pair in a calm atmosphere is predicted to dissipate very slowly. The vorticity distribution retains its shape initially (except for some slight vortex-on-vortex straining), and shows signs of trailing a wake after 20 vortex flow times. The vorticity level has dropped a factor of 10 below its initial value after 100 vortex flow times. For a typical landing B-747 aircraft, a flow time roughly corresponds to about 10 seconds. The apparent persistence of the vortex pair is not in agreement with observation.

A substantial increase in the decay rate occurs when the pair is placed in a turbulent flowfield. We assume that the turbulence is the result of a headwind

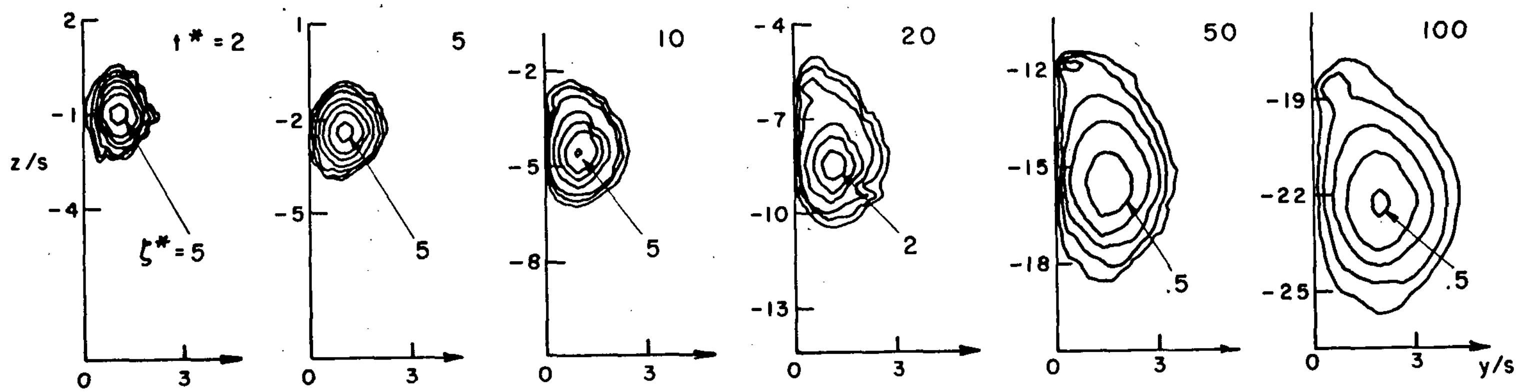

Figure 2. Isopleths of vorticity for a vortex pair descending in a calm neutrally stable atmosphere. Maximum contour values are given with subsequent values taken from 5, 2, 1, .5, .2, .1, .05, .02, .01, .005.

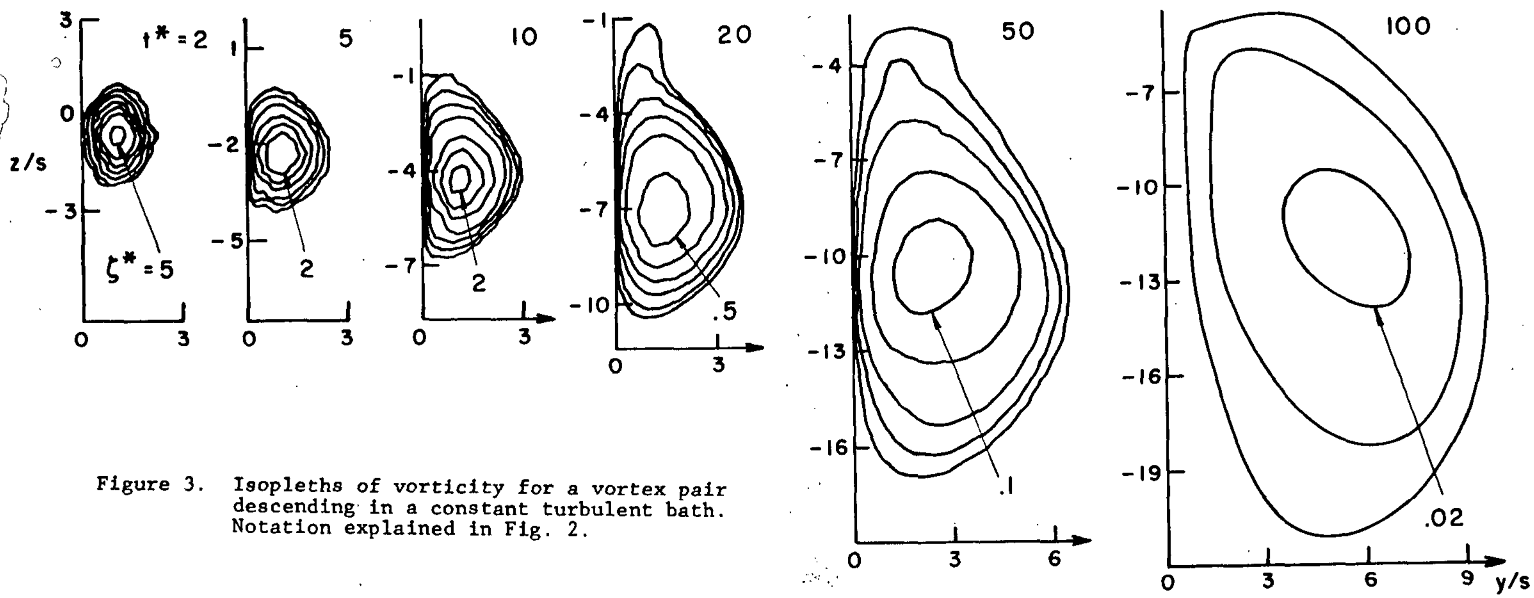

Figure 3. Isopleths of vorticity for a vortex pair descending in a constant turbulent bath. Notation explained in Fig. 2.

gradient, $\partial U/\partial z$, such that the background turbulent level through (2) is nonzero and homogeneous.

If the scale length is taken to be $\Lambda/s = 0.2$ and $(\partial U/\partial z)/(\Gamma_o/2\pi s^2) = 0.56$ the dissipation rate, $(2\pi)^3 s^4 \varepsilon/\Gamma_o^3 = 0.0025$ is obtained. Isopleths of vorticity are shown in Fig. 3. In comparison with Fig. 2, it can be seen that substantial diffusion of the vorticity has occurred, with a drop in maximum value of an order-of-magnitude below the zero background case. In addition, the structure of the vortex pair has been noticeably altered. It is clear from the shape of the isopleths at times greater than $t\Gamma/2\pi s^2 = 20.0$ that the vortex pair leaves a wake of low intensity vorticity. An extrapolation of the decay of the pair without background turbulence shows that over 10^4 flow times must pass before the zero background pair would decay to the same level as this decayed pair in 100 flow times.

Two quantities have been selected to quantify the amount of decay which occurs in a vortex pair; the circulation in a given area, and an integral which is approximately proportional to the rolling moment induced on a constant chord airfoil of semispan s_f. In Fig. 4 is shown the

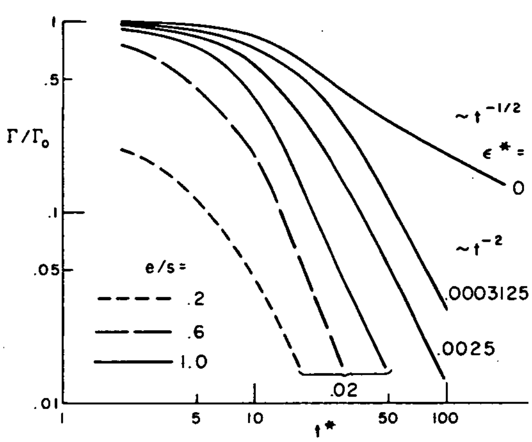

Figure 4. Circulation dropoff as a function of time for square contours of size $2e \times 2e$ centered on the local maximum of vorticity for several background dissipation ratio $\varepsilon^* = (2\pi)^3 s^4 \varepsilon/\Gamma_o^3$.

circulation computed about a square contour of dimension $2e \times 2e$ centered on the maximum of vorticity. The rate of decay as measured by Γ is independent of dissipation rate for sufficiently large times. These computations suggest that $\Gamma \sim t^{-2}$, which is expected from simple diffusion arguments that treat vorticity as passive tracer. Curiously the $\varepsilon = 0$ computation has a long time decay of $\Gamma \sim t^{-1/2}$. This time behavior may be shown to be the diffusion limit of a turbulent decaying pair once mean fluid convection of vorticity is neglected. As a general expected observation, when the integral scale is initialized to be the same between turbulent atmospheres of differing dissipation rate at comparable times after wake initialization, increased ε results in decreased circulation computed over a fixed contour. By far, however, it is our inability to quantify Λ in the atmosphere which precludes deriving a general decay curve for neutral turbulent atmospheres.

Corresponding rolling moment predictions for a follower aircraft, having a coaxial encounter with the vortex, are given in Fig. 5. Here the rolling moment

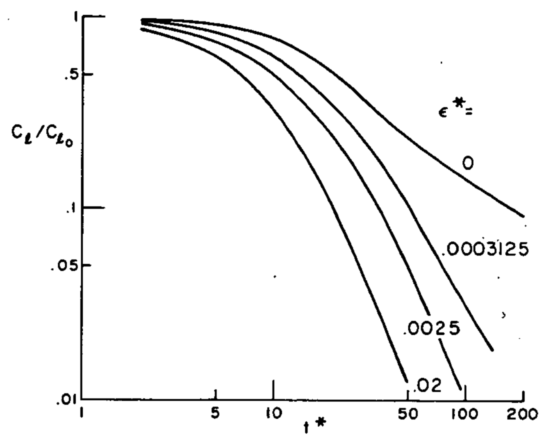

Figure 5. Rolling moment dropoff as a function of time for a follower aircraft of semispan $s_f/s = 1$ having a coaxial vortex encounter within several background dissipation rates $\varepsilon^* = (2\pi)^3 s^4 \varepsilon/\Gamma_o^3$.

is proportional to

$$C_{\ell\alpha} \int_{y_c - s_f}^{y_c + s_f} W(z_c, y)\,(y - y_c)\,dy \qquad (3)$$

and y_c and z_c are chosen so as to maximize the integral at a given time. Typically y_c and z_c are near the maximum in vorticity. The rolling moment curves for smaller follower aircraft are within 10 percent of the curves shown at these ε levels, and are thus fairly represented by the $s_f/s = 1$ curves. Again, the rolling moment curve decays as $t^{-1/2}$ for the calm atmosphere and as t^{-2} for the turbulent atmosphere.

IV. A Vortex Pair Subjected to a Cross Flow Shear

Tombach[9] has observed during aircraft

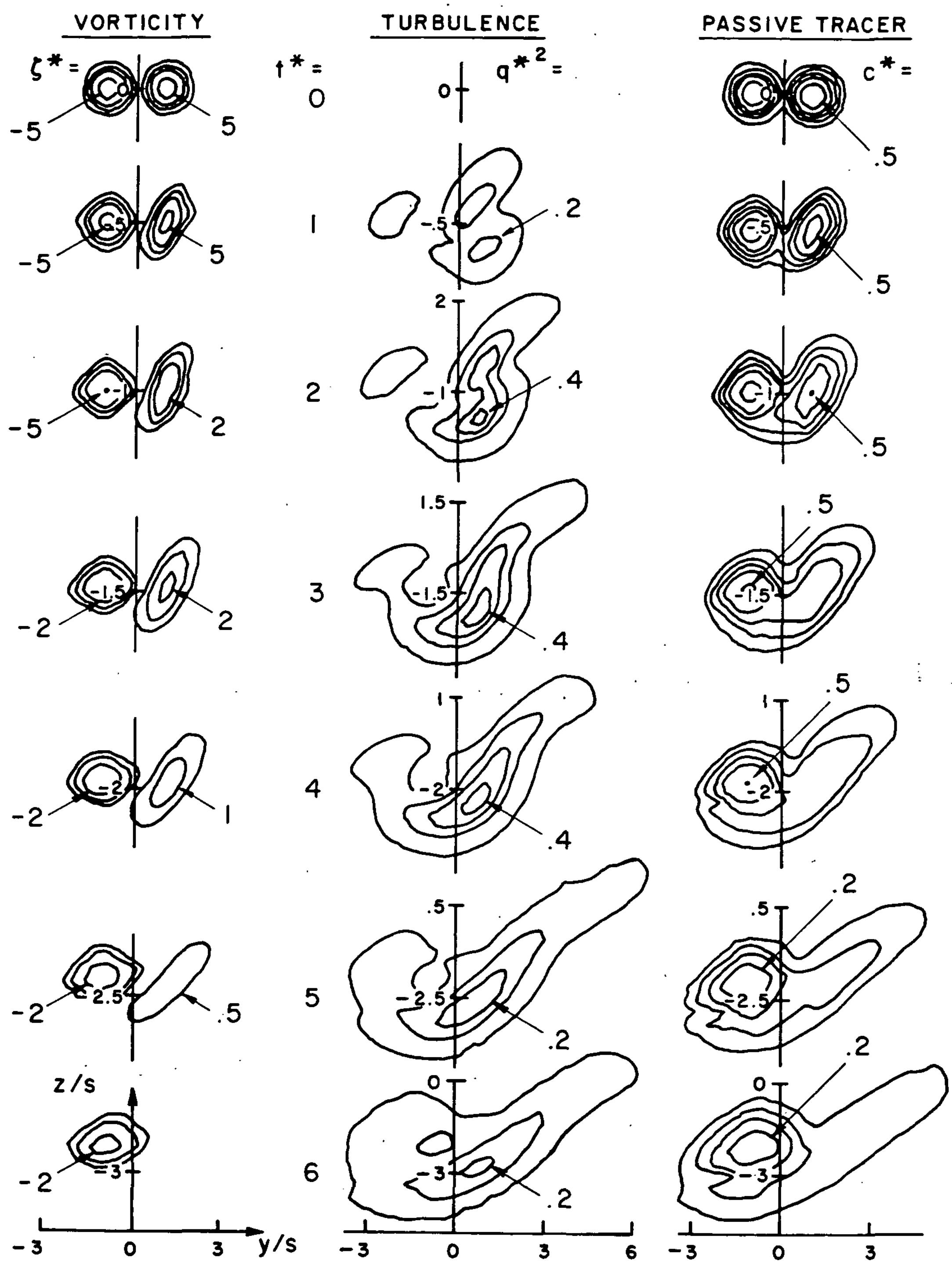

Figure 6. Isopleths of vorticity of a vortex pair subjected to a cross shear. Values are ±5, ±2, ±1, ±.5 .
Figure 7. Isopleths of turbulence for the pair in cross shear. Values .4, .3, .2, .1 .
Figure 8. Isopleths of tracer for the pair in cross shear. Values .5, .2, .1, .05, .02 .

flight tests that under certain atmospheric conditions the smoke in one vortex would vanish while the second vortex remained intact. This phenomenon has come to be called the solitary vortex phenomenon. At the time of observation, it was conjectured that atmospheric shear might be responsible in some way. More recently, Rossow[10] using distributions of point vortices has shown that a vortex immersed in a cross shear is rapidly distorted when the shear is of opposite sign of the vorticity. Computations were undertaken to see if the large distortion in vortex structure could generate turbulence and thereby diffuse the smoke seeded in the vortex to make it visible.

The computation was initialized, as in Fig. 1, but now a cross shear of magnitude $\beta = (\partial V/\partial z)/(2\pi s^2/\Gamma_o) = 0.5$ was imposed. Figures 6 and 7 show isopleths of vorticity and turbulence. The vortex of sign opposite to the cross shear is distorted which results in an increased turbulent level inside the vortex. Figure 8 is the computed dispersion of passive tracer which results. The fluid mechanisms which result in the enhanced dispersion of smoke in one vortex are now clear. It is concluded that it is cross wind that is responsible for the phenomenon of the solitary vortex.

To quantify the decay of vortices in cross shear, the rolling moment was computed and is shown in Fig. 9. Note that

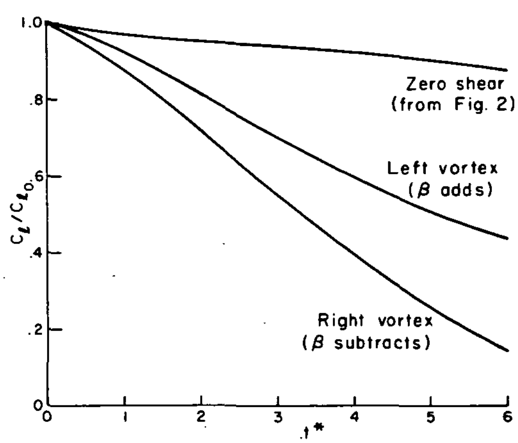

Figure 9. Rolling moment dropoff as a function of time for a follower aircraft of semispan $s_f/s = 1$ having a coaxial encounter. Normalized constant cross shear is $\beta = 0.5$.

the rolling moment induced by the right vortex is about half that induced by the left vortex at six flow times. As can be seen at six flow times, both the right and left vortices induce rolling moments on a follower aircraft which are well below the rolling moments induced by the same vortex pair in a calm atmosphere. This general enhanced decay in the left vortex, is attributed to the turbulent diffusion associated with the cross shear. It has been speculated that in the atmosphere over periods of tens of minutes it is possible to have shear with turbulence when the atmosphere is stably stratified. One might speculate that under these conditions the solitary vortex may indeed persist for long periods of time.

V. Vortex Pair in Ground Effect

One of the most perplexing observations of vortices has been the rebounding of a vortex as it approaches the ground. The phenomenon, we believe, was first observed by Dee and Nicholas [11] in 1968 and has been observed numerous times by researchers measuring vortex trajectories at airports.[12] In 1971 Harvey and Perry,[13] prompted by the above observation, conducted a series of tests in a wind tunnel with a moving floor to simulate correctly the ground plane. Using total head probes they concluded that the proximity of the vortex to the ground plane could result in boundary layer separation and secondary vorticity which could explain the upward migration of the vortex pair.

The computer code was modified to include a viscous ground plane in an effort to simulate the ground interaction. The surface is fixed at a level plane $z = z_o$ (where z_o is the roughness height). As far as the streamfunction boundary conditions are concerned, this surface is merely another reflecting plane across which oppositely-signed image vortices influence the flow (much as the image vortex of strength $-\Gamma_o$ did in Sections III and IV). The vortex pair will be assumed sufficiently close to the surface so that the velocity gradient, $\partial U/\partial z$, maintaining a small turbulence level, may be taken to be inversely proportional to z. Since the scale length is proportional to z in the Monin-Obukhov sublayer, the background turbulence level may still be taken constant. All necessary turbulence quantities, however, will be given zero vertical gradients at the hydrodynamic roughness height. We relate the vorticity level at the surface to the streamfunction there by a finite difference representation of the Poisson equation and the velocity law-of-the-wall to give:

$$\eta = -\frac{2(\psi_+ - \psi_r)}{(\Delta z)^2\left[1 + \frac{2z_r \ln(z/z_o)}{\Delta z}\right]} \qquad (4)$$

where ψ_+ is the streamfunction value at $z_+ = z_r + \Delta z$, and z_r is the reference z height above z_o (typically $z_r/s = 0.01$). When the flow simulation begins, (4) gives an immediate surface vorticity layer of opposite sign to the vortex convecting toward the surface from above. A sequence of contour plots of vorticity for the case where $z_0/s = 10^{-4}$, with the vortices initially positioned at $y/s = \pm 1$, $z/s = 2$, is shown in Fig. 10.

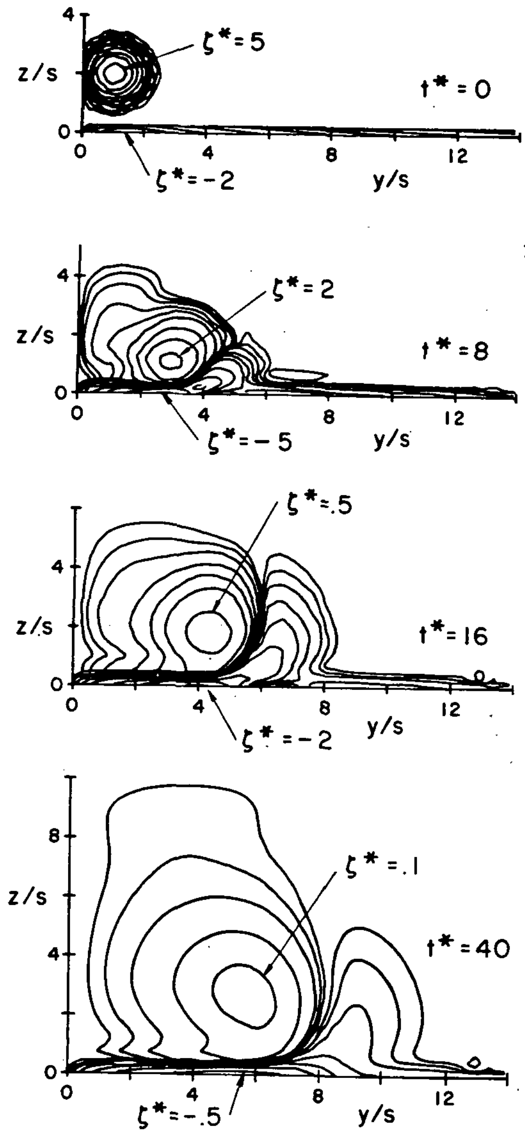

Figure 10. Isopleths of vorticity for a vortex pair descending toward a ground plane. Positive contours around the vortex follow from the given maximum values as given in Fig. 2. Negative contours generated near the wall follow -5, -2, -1, -.05, -.02, -.01, -.005.

As the vortex approaches the ground (its pair is across the reflecting plane at $y = 0$), the boundary layer beneath grows and separates, resulting in a secondary vortex. The secondary vortex is of the opposite sign to the descending vortex around which it is advected. The secondary vortex induces an upward and outward motion on the descending vortex pair, which results in a rebound (bounce) of the pair away from the ground plane. The rebound phenomenon described here suggests that the classical "inviscid" description of a pair of vortices following a hyperbolic trajectory may not be a particularly good model. In Fig. 11 is shown the computed trajectories of the maximum value of passive tracer.

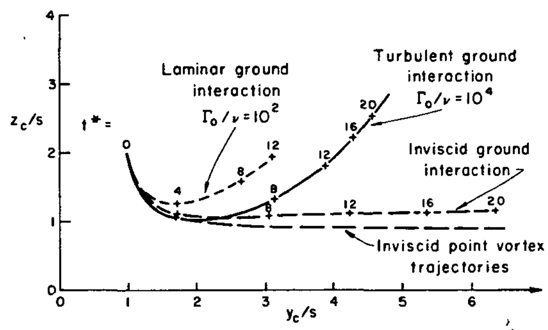

Figure 11. Trajectories of the maximum value of passive tracer carried by a vortex pair descending onto a ground plane.

Note that a laminar computation has been undertaken at $\Gamma_0/\nu = 100$ and the rebounding phenomenon still occurs.

Curiously, Barker and Crow [14] have recently investigated vortex pairs in ground effect and have attributed the rebound to effects of finite vortex core radius. To demonstrate that this explanation is suspect, we have undertaken a computation with an inviscid boundary condition applied on the ground (vanishing of vertical velocity). The vortex spread, $\sigma = 0.5$, is used and the results of the computation are summarized also in Fig. 11. As can be seen the rebounding phenomenon does not occur unless the viscous boundary condition is applied, even though the vortex cores are of finite size. It is seen that the finite difference solution with inviscid ground plane is in good agreement with the hyperbolic point vortex trajectories. The slight drift upward results from diffusion of the smoke.

The decay which results from scrubbing along a viscous ground is presented in Fig. 12. Included is the rolling moment decay curve with zero background turbulence taken from Fig. 5.

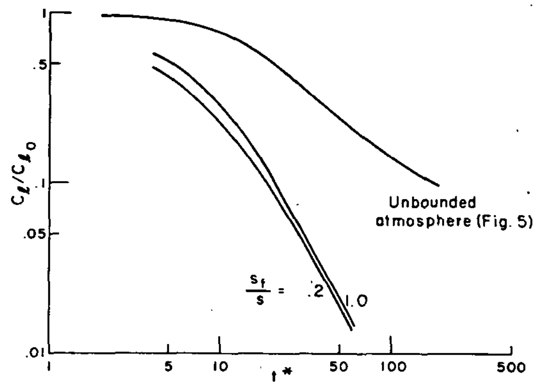

Figure 12. Rolling moment dropoff as a function of time for follower aircraft having coaxial encounters with a vortex interacting with the ground.

As can be seen, interaction with the ground provides a mechanism which greatly reduces the rolling moment induced on a follower aircraft over that induced by the same vortex pair left to decay out of ground effect.

VI. Conclusions

Two-dimensional aircraft trailing vortex pairs descending in a neutral atmosphere are shown to have enhanced dispersion when the atmosphere is turbulent, when cross wind shears are present and when the vortices interact with the ground. These results are predictions from the finite difference computer code, "VORTEX WAKE," which uses second-order closure turbulent modeling to include turbulent transport. In particular, the following conclusions are drawn with regard to neutral atmospheres:

1) The decay of a vortex pair immersed in a turbulent bath is enhanced with increasing dissipation rate providing the integral scale of the turbulence remains constant. In general, however, the dissipation rate, even in neutral atmospheres, is insufficient to quantify dispersing effectiveness of the atmosphere.

2) The phenomenon of the solitary vortex is shown to result as a consequence of cross wind shear. The vortex having the sign of vorticity opposite that of the vorticity in the shear is convectively distorted, producing turbulence in the vortex. This turbulence then disperses the smoke which was introduced in the vortex for visualization purposes.

3) The classic inviscid notion that a vortex pair descending towards a ground plane follows a trajectory that is hyperbolic is generally not correct. The vortex pair rebounds or bounces away from the ground as a result of separation of the ground boundary layer below the vortex. It is shown that this separation results in secondary vortices which induce a velocity on the descending vortices outward and upward, thereby explaining the rebounding phenomenon. It is speculated that when cross winds are present symmetries of the secondary vortices are destroyed. This results in tipping of the descending pair which has been observed.

Acknowledgement

This work was sponsored by NASA, Langley Research Center under contract No. NAS1-14707.

References

1. Donaldson, C. duP. and Bilanin, A.J.: "Vortex Wakes of Conventional Aircraft," AGARDograph No. 204, May 1975.

2. Hallock, J. N. and Eberle, W.R.: "Aircraft Wake Vortices: A State-of-the-Art Review of the United States R&D Program," FAA Report No. FAA-RD-77-23, February 1977.

3. Bilanin, A. J., Teske, M. E. and Williamson G. G.: "Vortex Interactions and Decay in Aircraft Wakes," *AIAA Journal*, Vol. 15, No. 2, February 1977, pp. 250-260.

4. Rossow, V. J.: "Inviscid Modeling of Aircraft Trailing Vortices," Proceedings, NASA Symposium on Wake Vortex Minimization, Washington DC, Feb. 25-26, 1976, pp. 4-54.

5. Donaldson, C. duP.: "Atmospheric Turbulence and the Dispersal of Atmospheric Pollutants." *AMS Workshop on Micrometeorology* (D.A. Haugen, ed.), Science Press, pp. 313-390.

6. Lewellen, W. S. and Teske, M. E.: "Turbulence Modeling and Its Application to Atmospheric Diffusion," EPA-600/4-75-016, 1975.

7. Swarztrauber, P. and Sweet, R.: "Efficient Fortran Subprograms for the Solution of Elliptic Partial Differential Equations," NCAR-TN/IA-109, 1975.

8. Arakawa, A.: "Numerical Simulation of Large-Scale Atmospheric Motions in Numerical Solution of Field Problems in Continuum Physics," SIAM-AMS Proceedings, Vol. II, 1970, pp. 24-40.

9. Tombach, I., "Observations of Atmospheric Effects of Vortex Wake Behavior," *AIAA Journal Aircraft*, Vol.

10, No. 11, Nov. 1973, pp. 641-647.

10. Rossow, V. J.: "Convective Merging of Vortex Cores in Lift-Generated Wakes," AIAA Paper No. 76-415, AIAA 9th Fluid and Plasma Dynamics Conference, San Diego, Calif., July 14-16, 1976.

11. Dee, F.W. and Nicholas, O.P.: "Flight Measurements of Wing Tip Vortex Motion Near the Ground," CP1065, British Aeronautical Research Council, London. 1968.

12. Bradshears, M. R., Logan, N. A. and Hallock, J. N.: "Effect of Wind Shear and Ground Plane on Aircraft Wake Vortices," *AIAA Journal Aircraft*, Vol. 12, No. 10, October, 1975, pp. 830-833.

13. Harvey, J.K. and Perry F.J.: "Flow-field Produced by Trailing Vortices in the Vicinity of the Ground," *AIAA Journal*, Vol. 9, No. 8, pp. 1659-1660. 1971.

14. Barker, S. J. and Crow, S. C.: "The Motion of Two-Dimensional Vortex Pairs in a Ground Effect," *Journal Fluid Mechanics* Vol. 82, part 4, 1977, pp. 659-671.

REFERENCES

1. Bilanin, A.J., Teske, M.E., Donaldson, C. duP., and Williamson G.G.: "Vortex Interactions and Decay in Aircraft Wakes." NASA CR-2870, September 1977.

2. Lewellen, W.S., Teske, M.E., and Donaldson, C. duP.: "Turbulence Model of Diurnal Variations in the Planetary Boundary Layer." *Proceedings of the 1974 Heat Transfer and Fluid Mechanics Institute,* (L.R. Davis and R.E. Wilson (Eds.)), Stanford U. Press, 1974.

3. Lewellen, W.S., and Teske, M.E.: "Prediction of the Monin-Obukhov Similarity Functions from an Invariant Model of Turbulence." *Journal of Atmospheric Sciences,* Vol. 30, No. 7, October 1973, pp. 1340-1345.

4. Lewellen, W.S., and Teske, M.E.: "Second-Order Closure Modeling of Diffusion in the Atmospheric Boundary Layer." *Boundary-Layer Meteorology* , Vol. 10, 1976, pp. 69-90.

5. Lewellen, W.S.: *"Use of Invariant Modeling."* Handbook of Turbulence Vol. 1, (Edited by W. Frost and T. H. Moulden) Plenum Publishing Corp., 1977.

6. Donaldson, C. duP.: "The Relationship Between Eddy Transport and Second-Order Closure Models for Stratified Media and for Vortices." A.R.A.P. Report No. 180, July 1972.

7. Bilanin, A.J., Teske, M.E., and Hirsh, J.E.: "A Look at the Deintensification that Results as a Consequence of Vortex Breakdown." Presented at the Aircraft Wake Vortices Conference, Boston March 1977. DOT publication No. FAA-RD-77-68. A.R.A.P. Report No. 305.

8. Bilanin, A.J., and Hirsh, J.E.: "Application of Second-Order Turbulent Modeling to the Prediction of Radiated Aerodynamic Sound." A.R.A.P. Report No. 308, June 1977.

9. Swarztrauber, P., and Sweet, R.: "Efficient Fortran Subprograms for the Solution of Elliptic Partial Differential Equations," NCAR-TN/IA-109, 1975.

10. Tombach, I.: "Observations of Atmospheric Effects of Vortex Wake Behavior." *AIAA Journal Aircraft,* Vol. 10, No. 11, November 1973, pp. 641-647.

11. Saffman, P.G.: "The Motion of a Vortex Pair in a Stratified Atmosphere." *Studies in Applied Mathematics,* Vol. Ll, No. 2, June 1972.

12. Tombach, I.H.: "Transport of a Vortex Wake in a Stably Stratified Atmosphere." *Aircraft Wake Turbulence and its Detection*, (Edited by J. H. Olsen, A. Goldburg and M. Rogers) Plenum Press, New York, 1971. pp. 41-57.

13. Tulin, M.P., and Schwartz, J.: "The Motion of Turbulent Vortex Pairs in Homogeneous and Density Stratified Media." Presented at the 8th O.N.R. Symposium on Naval Hydrodynamics, California Institute of Technology, August 1970.

14. Crow, S.C.: "Motion of a Vortex Pair in a Stably Stratified Fluid." Poseidon Research Report No. 1, May 1974.

15. Narain, J.P., and Uberoi, M.S.: "The Motion of a Trailing Vortex Wake in a Stratified Medium." *Atmospheric Environment*, Vol. 8, pp. 459-473. 1974.

16. Widnall, S.E.: "The Structure and Dynamics of Vortex Filaments." *Annual Review of Fluid Mechanics*, Vol. 7, 1975.

17. Donaldson, C. duP., and Bilanin, A.J.: "Vortex Wakes of Conventional Aircraft." AGARD-AG-204, May 1975.